



Supplement of

Sea salt reactivity over the northwest Atlantic: an in-depth look using the airborne ACTIVATE dataset

Eva-Lou Edwards et al.

Correspondence to: Armin Sorooshian (armin@arizona.edu)

The copyright of individual parts of the supplement might differ from the article licence.

21 **S1. Additional information for Equations 1 - 5**

22 Equations 1 – 4 comprise a system of four equations for determining the contribution of sea
23 salt and dust to bulk PILS Na^+ and Ca^{2+} mass concentrations. Equation 5 (derived from Eqs. 1 –
24 4) can produce negative values for ssNa^+ depending on $\text{Na}^+_{\text{bulk}}$ and $\text{Ca}^{2+}_{\text{bulk}}$. In these cases, ssNa^+
25 is set to 0, which prevents negative mass concentrations from also being assigned to $\text{Na}^+_{\text{dust}}$, ssCa^{2+} ,
26 and $\text{Ca}^{2+}_{\text{dust}}$.

27 **S2. Additional information for Equations 6 - 14**

28 Equations 6 – 13 constitute a system of equations for determining the contribution of sea salt,
29 dust, and emissions from combustion processes to bulk PILS Na^+ , Ca^{2+} , and K^+ mass
30 concentrations. When a computer-based solver attempts to solve Eqs. 6 – 13, nonphysical results
31 are often produced (i.e., either negative mass concentrations arise for certain species or there is no
32 solution at all). Thus, we manually solve for one unknown variable at a time and adjust calculated
33 values as necessary to arrive at a physical solution using the following method:

- 34 1. Manual calculations begin with Eq. 14 (derived from Eqs. 6 – 13), yet Eq. 14 can produce
35 negative values for ssNa^+ depending on $\text{Na}^+_{\text{bulk}}$, $\text{Ca}^{2+}_{\text{bulk}}$, K^+_{bulk} , and the selected
36 $\left(\frac{\text{Na}^+}{\text{K}^+}\right)_{\text{comb}}$. In these cases, ssNa^+ is set to 0, which prevents negative mass concentrations
37 from also being assigned to ssCa^{2+} and ssK^+ via Eq. 9 and 11, respectively.
- 38 2. If ssCa^{2+} and ssK^+ exceed $\text{Ca}^{2+}_{\text{bulk}}$ and K^+_{bulk} , respectively, ssCa^{2+} and ssK^+ are set to
39 $\text{Ca}^{2+}_{\text{bulk}}$ and K^+_{bulk} , respectively.
- 40 3. If the sum of K^+_{dust} and ssK^+ exceed K^+_{bulk} , K^+_{dust} is set to $\text{K}^+_{\text{bulk}} - \text{ssK}^+$, which forces K^+_{comb}
41 to be 0.
- 42 4. If the sum of $\text{Na}^+_{\text{comb}}$ and ssNa^+ exceed $\text{Na}^+_{\text{bulk}}$, $\text{Na}^+_{\text{comb}}$ is set to $\text{Na}^+_{\text{bulk}} - \text{ssNa}^+$, which
43 forces $\text{Na}^+_{\text{dust}}$ to be 0. Note that this adjustment prioritizes allotment of $\text{Na}^+_{\text{bulk}}$ to $\text{Na}^+_{\text{comb}}$
44 over $\text{Na}^+_{\text{dust}}$. We performed this same adjustment except prioritizing assignment of $\text{Na}^+_{\text{bulk}}$
45 to $\text{Na}^+_{\text{dust}}$ over $\text{Na}^+_{\text{comb}}$, and it did not significantly alter our results.

Table S1. Nomenclature for variables used in calculations relevant to Cl⁻ depletion.

Variable(s)	Description
$Na_{bulk}^+, Ca_{bulk}^{2+}, K_{bulk}^+, SO_4^{2-}_{bulk}, NO_3^-_{bulk}, oxalate_{bulk}, Cl_{bulk}^-$	Raw mass concentrations for each of the species listed from PILS-IC analysis. ¹
$NH_4^+_{bulk}$	Raw mass concentrations of NH ₄ ⁺ from the AMS ² .
$ssNa^+, ssCa^{2+}, ssK^+$	Derived mass concentrations attributed to sea salt for each of the species listed.
$Na_{dust}^+, Ca_{dust}^{2+}, K_{dust}^+$	Derived mass concentrations attributed to dust for each of the species listed.
Na_{comb}^+, K_{comb}^+	Derived mass concentrations attributed to combustion processes for each of the species listed.
<i>Sea salt</i>	Derived mass concentrations of sea salt.
$\%Cl^- \text{ depletion}$	Derived percentages of the original Cl ⁻ in sea salt particles that has since been displaced through depletion reactions.
<i>Lost Cl⁻</i>	Derived mass concentrations of particulate Cl ⁻ displaced from sea salt particles (when reported in units of $\mu\text{g m}^{-3}$) or the molar fraction of gaseous Cl added to the atmosphere following Cl ⁻ depletion reactions (when reported in units of pptv or ppbv). Note these are equivalent. Values are calculated using Approach 1, meaning that non-sea salt sources of Na ⁺ are considered.
<i>Lost Cl⁻_{bulk}</i>	Same as lost Cl ⁻ above, but calculated using Approach 2, meaning that sea salt is assumed to be the only source of atmospheric Na ⁺ .
<i>Lost Cl⁻_{diff}</i>	Difference between lost Cl ⁻ _{bulk} and lost Cl ⁻ , which is used to understand how assumptions about the source(s) of atmospheric Na ⁺ affect derived amounts of displaced Cl ⁻ .
$nssSO_4^{2-}$	Derived mass concentrations of SO ₄ ²⁻ attributed to sources other than sea salt.
$ExSO_4^{2-}, ExNO_3^-$	Derived mass concentrations of SO ₄ ²⁻ and NO ₃ ⁻ , respectively, remaining after neutralization with NH ₄ ⁺ .
$ExNH_4^+$	Derived mass concentrations of remaining NH ₄ ⁺ after neutralizing nssSO ₄ ²⁻ .
<i>Excess acidic species</i>	Derived total mass concentrations of the acidic species not neutralized by ammonium and, thus, having the potential to displace Cl ⁻ from sea salt particles.
<i>Lost Cl⁻ attr. to A</i>	Hypothetical mass concentrations of the amount of Cl ⁻ a given acidic species has the potential to displace, where A can be ExSO ₄ ²⁻ , Ex NO ₃ ⁻ , or oxalate _{bulk} .
<i>Lost Cl⁻ attr. to excess acidic species</i>	Hypothetical mass concentration of the total Cl ⁻ that can be displaced from sea salt particles based on the available amount of excess acidic species.

47 ¹“PILS-IC analysis” refers to in-flight sampling with a particle into liquid sampler (PILS)
48 following by offline sample analysis using ion chromatography (IC).

49 ²“AMS” stands for aerosol mass spectrometer.

50 **Table S2.** Mass ratios, molecular weights, and charges of fully deprotonated conjugate bases
 51 used in calculations relevant to Cl⁻ depletion.

Type of parameter	Parameter	Value
Mass ratio [unitless]	$\left(\frac{\text{total mass}}{Na^+}\right)_{ss}$	3.267 ^a
	$\left(\frac{Ca^{2+}}{Na^+}\right)_{ss}$	0.038 ^{b, c}
	$\left(\frac{Ca^{2+}}{Na^+}\right)_{dust}$	1.78 ^b
	$\left(\frac{K^+}{Na^+}\right)_{ss}$	0.036 ^{a, c}
	$\left(\frac{K^+}{Ca^{2+}}\right)_{dust}$	1.00 ^d
	$\left(\frac{Na^+}{K^+}\right)_{comb}$	See Table S2
	$\left(\frac{SO_4^{2-}}{Na^+}\right)_{ss}$	0.253 ^{e, f, g}
	$\left(\frac{Cl^-}{Na^+}\right)_{ss}$	1.81 ^b
Molecular weight [g mol ⁻¹]	$MW_{SO_4^{2-}}$	96.056
	$MW_{NH_4^+}$	18.039
	$MW_{NO_3^-}$	62.005
	MW_{Cl^-}	35.453
	$MW_{oxalate}$	88.019
Charge of fully deprotonated conjugate base [unitless]	$y_{SO_4^{2-}}$	2
	$y_{NO_3^-}$	1
	$y_{oxalate}$	2

52 ^aSeinfeld and Pandis (2016)

53 ^bBowen (1979)

54 ^cFinlayson-Pitts and Pitts (2000)

55 ^dAldhaif et al. (2020)

56 ^eBecagli et al. (2005)

57 ^fBoreddy and Kawamura (2015)

58 ^gFarren et al. (2019)

59 **Table S3.** Details regarding the various $\left(\frac{Na^+}{K^+}\right)_{comb}$ ratios used when exploring how different
 60 combustion processes may affect calculations relevant to Cl^- depletion.

Indicator used in text	Description of combustion process	Value
Herbaceous agricultural fire	Agricultural burning of herbaceous crop residue	0.05 ^a
Forest fire	Forest fire burning of pinion and juniper trees	0.08 ^b
Industrial (avg)	Average from industrial operations at steel mills and cement plants	0.24 ^{c, d}
Sauna stove	Inefficient batch combustion of birch wood in a sauna stove for residential heating	0.75 ^e
Car exhaust	Fossil fuel combustion by motor vehicles	0.91 ^{c, f}
Coal combustion (avg)	Average from burning of pulverized western coal comprised of low sulfur (0.5%) and high ash (22%) at a coal-fired power plant	3.03 ^{c, g}

61 ^aTurn et al. (1997)

62 ^bWatson et al. (2001)

63 ^cOoki et al. (2002)

64 ^dScheff and Valiozis (1990)

65 ^eLamberg et al. (2011)

66 ^fHuang et al. (1994)

67 ^gOndov et al. (1989)

68 **Table S4.** Summary of findings from this work as well as those from previous studies conducted around the globe. “BDL” stands for
 69 below detection limit, and “SSA” stands for sea salt aerosol. Several abbreviations are used and are defined as the following: “Ref” =
 70 reference, “Alt” = relevant altitudes, “Dp” = particle size range, “Stat” = statistic reported, “SSA” = sea salt aerosol, “Attr. Na⁺ to nss
 71 sources” = Attributes Na⁺ to non-sea salt sources, “Eq” = equation, “Air” = aircraft, “Surf” = surface station(s), “Med” = median, and
 72 “Rng” = range, “USEC” = United States East Coast, and “BDL” = below detection limit.

Ref	Date	Site	Platfo rm	Alt	D _p	Stat	SSA	Na ⁺	K ⁺	Ca ²⁺	Cl ⁻	Nss SO ₄ ²⁻	NO ₃ ⁻	NH ₄ ⁺	Cl: Na ⁺	Lost Cl ⁻	Cl ⁻ deple tion	Attr. Na ⁺ to nss sour ces	Eq/ method for determining SSA mass and/or Cl ⁻ depletion (%)	Eq/ method ref
This study	Dec- Feb 2022	USEC; 34.0°– 41.7° N/ 70.0°– 76.7° W	Air	160 – 200 0	< 5 ¹	Med	0.61 0.65 0.95 4.3	0.25 0.27 0.26 1.24	0.04 0.07 0.05 0.06	0.0 6 3 2	0.3 2	0.66 0.71 0.90 1.6	0.49 0.81 0.55 1.34	0.27 0.38 0.57 0.90	1.70 ² 1.62 ² 0.64 ² 1.35 ²	0.04/27 0.04/27 0.66/440 0.68/454	6 10 64 25	Yes	Eqs. 1 – 4, 15, 16	Boreddy and Kawamura (2015); AzadiAghdam et al. (2019)
Mar 2022	USEC; 32.2°– 38.5° N/ 69.1°– 76.5° W																			
May 2022	USEC; 32.3°– 41.7° N/ 69.1°– 76.5° W																			
Jun 2022	Bermud a; 30.8°– 35.9° N/ 59.5°– 65.9° W																			
Studies in open ocean environments																				
Prospe ro (1979)	Jun- Aug 1975	NWA; 34°–40° N/ 52°–60° W	Ship	15	< 30	Mean	4.41 ³ /									No	SSA = 3.252 · Na ⁺			
Spada et al. (2015)	1987 - 1996	New Zealand; 41.3°– 46.4° S/ 168.4° E– 176.5° W	Surf		No upp er limi t	Rng	~6 - 14									No	SSA = 1.47 · Na ⁺ + Cl ⁻	Quinn and Bates (2005)		
Keene et al. (1990)	Jul- Sep 1988	Bermud a	Ship	10- m tow er on ship	No upp er limi t	Mean				1.3 3					0.68/454		Multiplies Na ⁺ by ratio in seawater			

			Air	MB L	N/ A	Mean	~6	0.1 3	~3	0.34/227	No	$SSA = 3.262 \cdot Na^+$	Wilson (1975)			
Heintz enberg et al. (2000)	1990 - 1997	30°-45° N ⁵	Ship and air	MB L												
Shinoz uka et al. (2004)	Nov- Dec 1995	Tasmani a; 135°- 160° E/38°- 57° S	Air	< 200	< 3.5/ No upper limi t ⁶	Rng	0 - 8/ 9 - 40									
Keene and Savoie (1998)	Apr- May 1996	Bermud a; 32° N/64° W	Surf	28	0.5 5- 17	Rng		3.4 2- 8.2 6	0.10 - 1.36 ⁶	0.22 - 1.35/147 - 900			$SSA = 3.262 \cdot Na^+$	Keene et al. (1986); Wilson (1975)		
Quinn and Bates (2005)	Nov- Dec 1995	Souther n Ocean south of Australi a Sub- tropica northeas t Atlantic	Ship	18	< 10	Mean	0.77	BDL	0.03	BDL	0.01			$SSA = 1.47 \cdot Na^+$ + Cl^-		
	Jun- Jul 1997						0.30	BDL		0.20	0.08	0.03				
	Jan- Feb 1999	Tropical Atlantic					0.38 /0.43 8	BDL/ 0.01 ⁸	0.01/ 0.08 ⁸	0.02/ 0.06 ⁸	0.00/ 0.01 ⁸					
Quinn et al. (2001)	Jan- Feb 1999	Norther n hemisp here marine ⁹	Ship	18	< 1.1/ 1.1 - 10	Mean	0.22/ 8.00	0.00/ 0.01	0.15/ <0.00	0.01/ 0.23	0.03/ <0.00					Holland (1978)
		Souther n hemisp here marine tropics ⁹					0.08/ 6.40	0.00/ 0.00	0.52/ 0.07	<0.00 / 0.19	0.05/ <0.00					
		Souther n hemisp here marine temperat e ⁹					0.14/ 9.5	0.00/ 0.00	0.56/ 0.03	<0.00 / 0.14	0.04/ <0.00					
Boredd y and Kawa mura (2015)	Dec- Feb 2001 - 2012 Mar- May 2001 - 2012	Chichiji ma Island; 27.1 °N /142.2 °E	Surf	259	No upper limi t	Mean		4.12 0	0.05 ¹ 2 ¹⁰	0.1 7.1 0	3.06 2.97	0.78 0.84	0.19 0.23	1.75 1.67	Yes	Same system of equations as Eqs. 1-4 in this study

	Jun-Aug 2001							2.52	0.02 ¹ ₀	0.0 ⁴¹⁰ ₄	4.9	1.06	0.24	0.11	1.82 ¹ ₁
-	2012							3.62	0.05 ¹ ₀	0.0 ⁴¹⁰ ₂	7.1	1.31	0.43	0.11	1.98 ¹ ₁
-	Sep-Nov 2001														
-	2012														
Jiang et al. (2021)	Summer 2008 - 2016	Northwest Pacific; 31°– 51.3° N/ 122°– 173° E	Ship	Top deck of ship	Unspecified	Rng (Mean)	1.6 – 42.0 (11.7)					No	SSA = 3.256 · Na ⁺	Riley and Chester (1976)	
Feng et al. (2017)	Nov 2012/ 2013	Yellow Sea and Bohai Sea	Ship		0.0 1 - 18	Mean	3.8/4.0					8 % and 35 % for particles < 10 and < 1 μ m, respectively	SSA = 3.26 · Na ⁺	Manders et al. (2010)	
	Mar-Apr 2014	Yellow Sea and North Pacific					4.0								
	Mar-May 2015						2.5								
Murphy et al. (2019)	Jul-Aug 2016, Jan-Feb 2017	30°–45° N over Pacific Ocean	Air	160 - 150 0	0.1 8 - 3	Rng	~0.5 – 2.5					Yes ¹²	Method using ion mass spectra		

Studies in coastal locations

Keene et al. (1990)	Jul-Sep 1988	USEC	Ship	10-m tow er on ship	No upper limit	Mean		4.0 4		1.11/740	No	Multiplies Na ⁺ by ratio in seawater
			Air	MB L				0.4 5		0.79/527		

Wai and Tanner (2004)	1995 - 1999	Hong Kong; 22.3° N/114.1 ° E	Surf	77	< 10	1995 mean	2.32							Yes ¹³	Uses Na ⁺ as indicator of SSA		
Quinn et al. (2001)	Jan-Feb 1999	USEC ⁸	Ship	18	< 1.1/ 1.1/ 1.1 - 10	Mean	0.12/ 9.20	0.02/ <0.00	2.40/ 0.09	0.04/ 2.30	0.54/ <0.00			No	$SSA = 1.47 \cdot Na^+ + Cl^-$	Holland (1978)	
Quinn and Bates (2005)	Jan-Mar 1999 Mar-Apr 2001	Northern Indian Ocean East coast of Japan, Sea of Japan, East China Sea	Ship	18	< 10	Mean s	0.25/ 0.08 ¹ 4	BDL/ 0.01 ¹ 4	0.05/ 0.25 ¹ 4	0.04/ 0.07 ¹ 4	0.01/ 0.05 ¹ 4				$SSA = 1.47 \cdot Na^+ + Cl^-$		
							0.08/ 0.06 ¹ 5	BDL/ BDL 15	0.15/ 0.07 ¹ 5	0.07/ 0.03 ¹ 5	0.05/ 0.02 ¹ 5						
	Jul-Aug 2002	USEC; 33°-45° N				0.04	BDL	0.1 7		0.03	0.05	0.4 (< 1 μm)/ 0.8 (1 - 10 μm)					
Keene et al. (2004)	Jul-Aug 2002	USEC; 33°-44° N/ 68°-80° W	Ship	18	<25	Median			0.1 9	3.48	0.79	0.57		86	N/A	Uses Mg ²⁺ as reference for SSA	Keene et al. (1986)
Nolte et al. (2008)	May-Jun 2002	Tampa, Florida, USA; ~27.9° N, 82.5° W	Surf	Unspecifi ed	0.0 56 - 18	Mean or mg	1.41		1.6 6	3.76 ¹ 6	1.74	1.19	0.2 - 0.35 (< 1 μm)/ 0.35 - 0.9 (> 1 μm)	48	No	Cl ⁻ depletion (%) determined by deficit of Cl ⁻ /Na ⁺ ratio from 1.17	Stumm and Morgan (1981)
Yao and Zhang (2012)	Jun-Jul, Oct-Nov 2002	Kejimkujik, Nova Scotia; 44.4° N /65.2° W	Surf	5 m abo ve gro und	3.1 - 6.2	Rng sum mer/ fall	0.05 - 0.22/ 0.03 - 0.24						8 - 10 0/ 0 - 55	No	Uses Cl ⁻ :Na ⁺ ratio of 1.174 in sea water to determine Cl ⁻ depletion (%)	Zhuang et al. (1999)	
	Nov 2002 ¹⁷				0.0 48 - 18	Rng <1 μm /> 1 μm	BDL 0.07/ 0.72 -	1.04 - 2.92/ 0.11	0.02 - 0.18/ 0.69	0.31 - 0.91/ 0.02							
Keene et al. (2007)	Jul-Aug 2004	Appledore Island, Maine, USA;	Surf	43	0.3 9 - 18/ No upp	Med or rng	0.68		0.5 0	0.96 -	0.26 -	0.80 -	0.00 - 1.31/0 - 874	No ¹⁹	Uses Na ⁺ and Mg ²⁺ to determine SSA	Keene et al. (1986)	

Zhao and Gao (2008)	Jul-Sep 2006	Newark, New Jersey, USA; 40.7° N/74.2° W	Surf	20 m above ve gro und	0.0 56 – 18	er limi t ¹⁸	Mean		0.33 – 1.21	14 – 96	Yes ²⁰	For samples with Na ⁺ :Mg ²⁺ > 5, Na ⁺ is reference species for SSA	Finlayson-Pitts and Pitts (2000)
Corral et al. (2021)	Dec-Feb 2014	USEC; 25.4°–44.4° N/70.0°–82.1° W	Surf ²¹	-3 - 157	< 2.5	Rng of mean s across s 9 statio ns	0.24- 1.15 0.35 – 1.26			N/A	SSA = 1.81 · Cl ⁻	http://vista.cira.colostate.edu/Improve/reconstructed-fine-mass/	
	2018						0.15						
	Jun-Aug 2014						–						
	0.70												
	2018						0.19-						
	Sep-Nov 2014						1.09						
	2018												
Haskin s et al. (2018)	Feb-Mar 2015	USEC; ~28°–43° N/68°–85° W	Air	< 100	< 4.1	Med		Ove r oce an: 0.2 8 – 0.2 Ove r lan d: 0.1 2 – 0.1 5 ²²	Over ocean: 0.30/202 Over land: 0.08/53	No	Na ⁺ and Cl ⁻ are assumed to come exclusively from SSA	Junge and Werby (1958)	
Kloppe r et al. (2020)	Feb-Dec 2016 – 2017	Henties Bay, Namibia	Surf	30 < 10	Mean		10.2 0.41 0.7 3	13. 9 3.60 ² 3	0.23 0.21 1.35 (201 6)/ 1.34 (201 7)	Yes	Similar system of equations as Eqs. 1–4 in this study	Seinfeld and Pandis (2016)	
Azadi Aghda m et al. (2019)	Jul-Dec 2018	Quezon City, Philippines; 14.6° N/ 121.1° E	Surf	85 56 - 18 < 2.5	Rng 0.1 – 2.6 Rng of (P) mean s	0.20 – 1.48			21 – 91	Yes	Same as Eqs. 1–4, 15, 16 in this study; SSA = ssNa ⁺ + Cl ⁻	Becagli et al. (2005); Boreddy and Kawamura (2015); Farren et al. (2019)	
	Aug 2005												
	– Oct 2007												

M ₂ s) 2.5 — 10 (P M _{co} arse)	— 0.44 — 0.74 — 1.59	0.44 — 1.46	Method using ion mass spectra; SSA particles identified as having Na ⁺ :Mg ²⁺ ~10:1	Pilson (1998)
Studies at inland locations				
Bondy et al. (2017) Jun-2013 Centreville, Alabama, USA; 32.9° N/87.3° W	Surf 242 0.3 2 — 1.8	76 Yes ²⁴ % of S particles S identified as A having pa rti cl es ha d Cl - de pl eti on ≥ 90 %		

73 ¹Median values for NH₄⁺ are for particles 0.06 – 0.60 μm.

74 ²Ratios of Cl⁻:ssNa⁺ are reported instead of Cl⁻:Na⁺.

75 ³Geometric mean.

76 ⁴Arithmetic mean.

77 ⁵Heintzenberg et al. (2000) consider data from multiple field campaigns covering nearly all longitudes and latitudes (see Fig. 1 of their study) over ocean. Thus, means listed above represent the 30° – 45° N latitude band over ocean for the entire globe instead of a specific region.

80 ⁶Filters inside the aircraft sampled particles < 3.5 μm, while filters outside the aircraft did not have an upper limit for the size of particles sampled.

82 ⁷Ranges of NO₃⁻ mass concentrations are for particles > 1 μm, all other ranges are for the specified size range (0.55 – 17 μm).

83 ⁸In the tropical Atlantic, air masses influenced by biomass burning (BB) and African dust were sampled. Mean values for a given parameter are reported as A/B, where A and B correspond to values associated with BB- and dust-influenced air masses, respectively.

85 ⁹Regimes defined in Quinn et al. (2001). Note that ranges of longitude and latitude are not provided for these regimes, but that the research vessel traveled from Norfolk, VA, USA (36.9° N, 76.3° W) to Cape Town, South Africa (34.3° S, 18.4° E).

87 ¹⁰Boreddy and Kawamura (2015) report non-sea salt K⁺ and Ca²⁺.

88 ¹¹These Cl⁻:Na⁺ ratios are higher than those typically found in sea salt particles. Boreddy and Kawamura (2015) note that non-sea salt
89 sources of Cl⁻ contributed to their samples in summer (June – August) and fall (September – November).

90 ¹²Particles containing aluminum, barium, and other metals were deemed to not be sea salt particles and excluded from the analysis in
91 Murphy et al. (2019).

92 ¹³Wai and Tanner (2004) reported they “carefully examined their dataset” and determined there was negligible contribution of local
93 non-sea salt sources of Na⁺ (e.g., crustal, granitic) to total Na⁺.

94 ¹⁴In the northern Indian Ocean, air masses were categorized as having recent (<2 days) contact with either the Arabian or Indian
95 continent. Mean values for a given parameter are reported as A/B, where A and B correspond to values associated with air masses from
96 the Arabian and Indian continent, respectively.

97 ¹⁵On the east coast of Japan, Sea of Japan, and East China Sea, air masses were categorized as having recent (<2 days) contact with
98 either (i) Asian continental regions with known sources of pollution or (ii) Asian continental regions with known sources of pollution
99 and dust. Mean values for a given parameter are reported as A/B, where A and B correspond to values associated with air masses likely
100 affected by (i) Asian pollution and (ii) Asian pollution and dust, respectively.

101 ¹⁶Nolte et al. (2008) reported total SO₄²⁻ instead of nssSO₄²⁻.

102 ¹⁷Yao and Zhang (2012) provided speciated sub- and supermicron mass concentrations for three samples collected in November 2002
103 that had substantially high mass concentrations of Na⁺, nssSO₄²⁻, NO₃⁻, and NH₄⁺.

104 ¹⁸Aerosols were sampled using a cascade impactor (0.39 – 18 μm) as well as in bulk where no upper size limit is specified. Cl⁻ and NO₃⁻
105 mass concentrations correspond to the sum across all impactor stages, while Na⁺ and nssSO₄²⁻ mass concentrations correspond to the
106 bulk samples.

107 ¹⁹Keene et al. (2007) found good agreement between their measured ratios of Na⁺ to Mg²⁺ to those documented for sea salt. They
108 proceeded assuming all Na⁺ and Mg²⁺ originated from the surface ocean.

109 ²⁰Zhao and Gao (2008) used Na⁺:Mg²⁺ ratios to categorize samples as either from marine-dominated (Group 1; >5) or continental-
110 dominated (Group 2; < 5) air masses. Calculations and discussion regarding Cl⁻ depletion only consider data from Group 1.

111 ²¹Stations operated through the United States Environmental Protection Agency (U.S. EPA) Interagency Monitoring of Protected Visual
112 Environments (IMPROVE) network.

113 ²²Haskins et al. (2018) provided day and night median Cl⁻ mass concentrations for over ocean and over land. Above, we combine the
114 day and night medians as a range.

115 ²³Klopper et al. (2020) reported total SO₄²⁻ instead of nssSO₄²⁻.

116 ²⁴Bondy et al. (2017) note particles identified and analyzed as sea salt were unlikely to be influenced by dust as they had negligible
117 amounts of soil elements, such as Si and Al. Samples from July 4 and 5 were excluded to eliminate influence from fireworks.

118 **Table S5.** Number of data points considered in Figs. 1, 4, and S6 for each of the parameters
 119 presented for each of the seasonal/monthly categories.

Parameter	Dec-Feb	Mar	Mar transit	May	May transit	Jun Bermuda
Temperature	105781	83108	12806	34175	27427	19807
Relative humidity	105846	83098	12805	34175	27421	19803
Water vapor mixing ratio	105846	83098	12805	34175	27421	19803
Wind speed	75483	58823	7994	19826	12955	6477
CO	75523	58407	8545	23799	18745	10946
Na ⁺	275	246	48	113	106	81
K ⁺	218	217	47	60	43	52
Ca ²⁺	235	244	48	73	81	67
Cl ⁻	268	230	43	43	65	78
Cl ⁻ :Na ⁺	258	227	43	43	65	77
K ⁺ :Na ⁺	185	208	47	58	41	52
Ca ²⁺ :Na ⁺	202	220	48	64	75	66
SO ₄ ²⁻	342	276	48	136	116	81
NO ₃ ⁻	322	269	48	137	119	83
Oxalate	263	227	43	137	120	82
NH ₄ ⁺	2748	2385	403	1169	947	678
Excess acidic species	1372	1790	423	468	373	486
ssNa ⁺	202	220	48	64	75	66
Cl ⁻ :ssNa ⁺	154	175	36	33	52	63
Lost Cl ⁻ attributed to ExSO ₄ ²⁻	1258	1748	418	391	323	466
Lost Cl ⁻ attributed to ExNO ₃ ⁻	1212	1733	418	391	323	466
Lost Cl ⁻ attributed to oxalate	263	227	43	137	120	82
Lost Cl ⁻ based on ssNa ⁺	190	206	43	33	53	64
Lost Cl ⁻ attributed to excess acidic species	1385	1794	423	468	373	487
ExSO ₄ ²⁻	1258	1748	418	391	323	466
ExNO ₃ ⁻	1212	1733	418	391	323	466
<i>m/z</i> 44	2748	2385	403	1169	947	678
<i>m/z</i> 79	2748	2385	403	1169	947	678

120

121 **Table S6.** Seasonal/monthly median values for each of the parameters presented in Figs. 1, 4, and
 122 S6. Recall the median is represented as a solid red line in the center of each box.

Parameter	Units	Dec-Feb	Mar	Mar transit	May	May transit	Jun Bermuda
Temperature	°C	2.7	9.2	13.3	19.9	19.2	21.9
Relative humidity	%	52.6	50.5	46.6	64.2	61.6	80.8
Water vapor mixing ratio	ppm	3607.38	5585.31	6868.43	15798.90	15681.40	21605.40
Wind speed	m s ⁻¹	8.926	10.266	8.617	8.355	6.710	6.425
CO	ppm	0.1332	0.1404	0.1408	0.1246	0.1214	0.0813
Na ⁺		0.25	0.27	0.75	0.26	0.46	1.24
K ⁺		0.04	0.07	0.09	0.05	0.03	0.06
Ca ²⁺	μg m ⁻³	0.06	0.13	0.14	0.12	0.05	0.07
Cl ⁻		0.32	0.43	1.33	0.46	0.31	1.68
Cl ⁻ :Na ⁺		1.443	1.309	1.376	0.391	0.456	1.310
K ⁺ :Na ⁺	-	0.132	0.267	0.119	0.065	0.020	0.037
Ca ²⁺ :Na ⁺		0.261	0.412	0.219	0.233	0.075	0.050
SO ₄ ²⁻		0.63	0.74	1.08	0.53	0.72	1.63
NO ₃ ⁻		0.49	0.81	0.77	0.55	0.74	0.90
Oxalate		0.01	0.01	0.01	0.04	0.03	0.02
NH ₄ ⁺	μg m ⁻³	0.28	0.38	0.46	0.58	0.56	0.24
Excess acidic species		0.30	0.57	0.36	0.05	0.44	1.82
ssNa ⁺		0.19	0.20	0.71	0.29	0.63	1.32
Cl ⁻ :ssNa ⁺	-	1.536	1.560	1.617	0.645	0.471	1.354
Lost Cl ⁻ attributed to ExSO ₄ ²⁻		0.00	0.00	0.00	0.00	0.00	0.46
Lost Cl ⁻ attributed to ExNO ₃ ⁻		0.13	0.29	0.18	0.00	0.42	0.58
Lost Cl ⁻ attributed to oxalate		0.01	0.01	0.01	0.03	0.03	0.02
Lost Cl ⁻ based on ssNa ⁺	μg m ⁻³	0.04	0.04	0.11	1.76	1.33	0.66
Lost Cl ⁻ attributed to excess acidic species		0.17	0.34	0.21	0.04	0.26	1.14
ExSO ₄ ²⁻		0.00	0.00	0.00	0.00	0.00	0.63
ExNO ₃ ⁻		0.24	0.51	0.32	0.00	0.74	1.02
<i>m/z</i> 44		0.11	0.22	0.38	0.46	0.41	0.03
<i>m/z</i> 79		0.01	0.02	0.03	0.03	0.02	0.01

123

124

125 **Table S7.** Dates, quantity of samples, meteorological conditions, and derived contributions of sea
 126 salt and dust to bulk PILS Na^+ (ssNa^+ and $\text{Na}^{+}_{\text{dust}}$, respectively) and Ca^{2+} (ssCa^{2+} and $\text{Ca}^{2+}_{\text{dust}}$,
 127 respectively) mass concentrations for research flights (RFs) considered in each category. “N PILS
 128 samples” refers to the total number of PILS samples collected during clear conditions on the date
 129 indicated, while “N samples w/ derived species” refers to the number of these samples providing
 130 enough information to solve Eqs. 1 – 4 (i.e., samples providing mass concentrations of both $\text{Na}^{+}_{\text{bulk}}$
 131 and $\text{Ca}^{2+}_{\text{bulk}}$).

Category	Date	RF(s)	N PILS samples	N samples w/ derived species	Meteorological conditions and/or relevant notes	Median ssNa^+ ($\mu\text{g m}^{-3}$)	Median $\text{Na}^{+}_{\text{dust}}$ ($\mu\text{g m}^{-3}$)	Median ssCa^{2+} ($\mu\text{g m}^{-3}$)	Median $\text{Ca}^{2+}_{\text{dust}}$ ($\mu\text{g m}^{-3}$)
Dec-Feb	30 November 2021	94	7	7	Remains of post-frontal conditions	0.00	0.14	0.00	0.31
	01 December 2021	95	16	16	Prefrontal, high pressure; smoke in boundary layer near coast	0.03	0.23	0.00	0.47
	07 December 2021	96	5	5	Postfrontal, cold high pressure behind a strong cold front	0.07	0.11	0.00	0.20
	11 January 2022	100, 101	6	4	Cold high pressure, cold air outbreak (CAO) conditions	0.32	0.03	0.01	0.07
	12 January 2022	102, 103	33	17	Cold high pressure	0.09	0.01	0.00	0.03
	15 January 2022	104	3	2	Postfrontal	0.67	0.02	0.01	0.04
	18 January 2022	105	11	0	Low pressure moves offshore, sets up CAO conditions	NaN	NaN	NaN	NaN
	19 January 2022	107, 108	26	6	Short-lived high pressure	0.28	0.04	0.01	0.07
	24 January 2022	109, 110	26	9	Postfrontal, weak high pressure	0.16	0.04	0.00	0.07
	26 January 2022	111, 112	20	7	Postfrontal	0.35	0.02	0.01	0.04
	27 January 2022	113, 114	18	5	Cold high pressure	0.24	0.00	0.01	0.00
	01 February 2022	115	8	5	High pressure	1.07	0.01	0.03	0.03

	02 February 2022	116	17	6	High pressure	0.74	0.00	0.02	0.01
	03 February 2022	117, 118	15	5	High pressure	1.00	0.00	0.02	0.00
	15 February 2022	120, 121	34	21	Postfrontal conditions, cold high pressure	0.22	0.01	0.00	0.02
	16 February 2022	122, 123	21	18	Cold high pressure	0.17	0.04	0.01	0.08
	19 February 2022	124, 125	38	30	Weak postfrontal	0.09	0.02	0.00	0.05
	22 February 2022	126, 127	25	24	Prefrontal, high pressure	1.47	0.03	0.04	0.05
	26 February 2022	128, 129	16	15	Postfrontal	0.11	0.03	0.00	0.05
	Overall	345	202			0.19	0.03	0.01	0.06
Mar	02 March 2022	130	39	36	Postfrontal, high pressure	0.19	0.08	0.01	0.15
	03 March 2022	131, 132	71	57	Weak prefrontal	0.71	0.13	0.03	0.26
	04 March 2022	133, 134	42	37	Cold high pressure	1.62	0.02	0.04	0.04
	13 March 2022	138	8	6	Postfrontal, CAO conditions	0.05	0.03	0.00	0.06
	14 March 2022	139, 140	38	36	Late postfrontal, cold high pressure; smoke plume sampled from a woodland fire	0.10	0.03	0.00	0.05
	18 March 2022	141	14	12	Weak postfrontal	0.13	0.02	0.00	0.03
	26 March 2022	144, 145	29	19	Postfrontal; sampled dust, smoke, and potentially pollen	0.02	0.02	0.00	0.04
	28 March 2022	146	17	12	Postfrontal	0.02	0.02	0.00	0.04
	29 March 2022	147, 148	19	5	Postfrontal, high pressure, CAO conditions	0.06	0.03	0.00	0.05

	Overall		277	220		0.20	0.05	0.01	0.11
May	03 May 2022	149	15	12	Weak prefrontal; presence of smoke potentially from New Mexico	0.36	0.07	0.01	0.13
	05 May 2022	150, 151	18	11	Postfrontal	0.03	0.02	0.00	0.04
	16 May 2022	153, 154	39	7	Prefrontal to an approaching cold front yet also postfrontal to a departing band of precipitation	0.11	0.14	0.00	0.26
	17 May 2022	155	37	7	Postfrontal	0.08	0.00	0.00	0.00
	20 May 2022	158	28	27	Warm high pressure, southerly flow due to Bermuda high ² ; haze with potential sampling of bioaerosol	1.77	0.04	0.06	0.08
	Overall		137	64		0.29	0.03	0.01	0.07
Mar transit	22 March 2022	142, 143	48	48	High pressure, two days after a cold front and two days before another cold front	0.71	0.05	0.03	0.10
May transit	18 May 2022	156, 157	67	46	Postfrontal along East Coast, aircraft passed across the cold front on the way to Bermuda	0.58	0.01	0.02	0.02
	21 May 2022	159, 160	42	24	Warm high pressure, anticyclonic flow around Bermuda high	0.72	0.01	0.02	0.02
	31 May 2022	161	11	5	Postfrontal	0.19	0.01	0.01	0.02
	Overall		120	75		0.63	0.01	0.02	0.02
Jun Bermuda	02 June 2022	162, 163	4	3	Prefrontal	0.83	0.00	0.01	0.00
	03 June 2022	164	1	0	Prefrontal, tropical system approaching from the southwest	NaN	NaN	NaN	NaN
	05 June 2022	165	29	26	Could only fly in the morning due to approaching tropical cyclone (TC), TC departs 06 June 2022.	1.94	0.00	0.07	0.00
	07 June 2022	167	1	0	High behind departing TC	NaN	NaN	NaN	NaN
	08 June 2022	168, 169	2	1	High pressure behind TC, African dust known to be in domain	5.63	0.48	0.21	0.86
	10 June 2022	170	1	1	High pressure, isolated thunderstorms, African dust known to be in domain	2.28	0.00	0.06	0.00

	11 June 2022	172, 173	20	12	High pressure, African dust known to be in domain	0.63	0.08	0.02	0.18
	13 June 2022	174	25	23	High pressure, African dust known to be in domain but sampled away from dust for contrast	1.31	0.00	0.05	0.01
	Overall		83	66		1.32	0.01	0.05	0.01

132

¹Davis et al. (1997)

133 **Table S8.** Dates, quantity of samples, meteorological conditions, and derived contributions of sea
 134 salt, dust, and combustion emissions to bulk PILS Na^+ (ssNa^+ , $\text{Na}^+_{\text{dust}}$, and $\text{Na}^+_{\text{comb}}$, respectively)
 135 and K^+ (ssK^+ , K^+_{dust} , and K^+_{comb} , respectively) for RFs considered in each category. Combustion
 136 emissions are assumed to not be a source of Ca^{2+} , so only contributions of sea salt and dust to bulk
 137 PILS Ca^{2+} mass concentrations are reported (ssCa^{2+} and $\text{Ca}^{2+}_{\text{dust}}$, respectively). Here, agricultural
 138 burning of herbaceous crop residue is considered as the only combustion process contributing to
 139 $\text{Na}^+_{\text{comb}}$ and K^+_{comb} . “N PILS samples” refers to the total number of PILS samples collected during
 140 clear conditions on the date indicated, while “N samples w/ derived species” refers to the number
 141 of these samples providing enough information to solve Eqs. 6 – 13 (i.e., samples providing mass
 142 concentrations of $\text{Na}^+_{\text{bulk}}$, $\text{Ca}^{2+}_{\text{bulk}}$, and K^+_{bulk}).

Category	Date	RF(s)	N PILS samples	N samples w/ derived species	Meteorological conditions and/or relevant notes	Median ssNa^+ ($\mu\text{g m}^{-3}$)	Median $\text{Na}^+_{\text{dust}}$ ($\mu\text{g m}^{-3}$)	Median $\text{Na}^+_{\text{comb}}$ ($\mu\text{g m}^{-3}$)	Median ssCa^{2+} ($\mu\text{g m}^{-3}$)	Median $\text{Ca}^{2+}_{\text{dust}}$ ($\mu\text{g m}^{-3}$)	Median ssK^+ ($\mu\text{g m}^{-3}$)	Median K^+_{dust} ($\mu\text{g m}^{-3}$)	Median K^+_{comb} ($\mu\text{g m}^{-3}$)
Dec-Feb	30 November 2021	94	7	1	Remains of post-frontal conditions	0.00	0.16	0.00	0.00	0.41	0.00	0.06	0.00
	01 December 2021	95	16	14	Prefrontal, high pressure; smoke in boundary layer near coast	0.08	0.23	0.00	0.00	0.48	0.00	0.05	0.00
	07 December 2021	96	5	3	Postfrontal, cold high pressure behind a strong cold front	0.08	0.11	0.00	0.00	0.22	0.00	0.03	0.00
	11 January 2022	100, 101	6	3	Cold high pressure, cold air outbreak (CAO) conditions	0.33	0.03	0.00	0.01	0.08	0.01	0.01	0.00
	12 January 2022	102, 103	33	11	Cold high pressure	0.15	0.04	0.00	0.01	0.08	0.00	0.02	0.00
	15 January 2022	104	3	2	Postfrontal	0.67	0.02	0.00	0.01	0.04	0.01	0.00	0.00
	18 January 2022	105	11	0	Low pressure moves offshore, sets up CAO conditions	NaN	NaN	NaN	NaN	NaN	NaN	NaN	NaN
	19 January 2022	107, 108	26	6	Short-lived high pressure	0.28	0.04	0.00	0.01	0.07	0.01	0.05	0.06
	24 January 2022	109, 110	26	9	Postfrontal, weak high pressure	0.17	0.04	0.00	0.00	0.07	0.01	0.05	0.02
	26 January 2022	111, 112	20	7	Postfrontal	0.33	0.02	0.01	0.01	0.04	0.01	0.03	0.35

	27 January 2022	113, 114	18	4	Cold high pressure	0.28	0.00	0.00	0.01	0.00	0.01	0.00	0.00
	01 February 2022	115	8	4	High pressure	1.08	0.01	0.00	0.02	0.03	0.02	0.00	0.00
	02 February 2022	116	17	4	High pressure	0.74	0.00	0.00	0.02	0.01	0.03	0.00	0.02
	03 February 2022	117, 118	15	4	High pressure	1.16	0.00	0.00	0.03	0.00	0.04	0.00	0.01
	15 February 2022	120, 121	34	7	Postfrontal conditions, cold high pressure	0.11	0.04	0.00	0.00	0.13	0.00	0.02	0.00
	16 February 2022	122, 123	21	10	Cold high pressure	0.13	0.06	0.00	0.00	0.12	0.00	0.04	0.00
	19 February 2022	124, 125	38	18	Weak postfrontal	0.06	0.02	0.00	0.00	0.11	0.00	0.04	0.00
	22 February 2022	126, 127	25	20	Prefrontal, high pressure	1.68	0.03	0.00	0.04	0.07	0.04	0.00	0.00
	26 February 2022	128, 129	16	14	Postfrontal	0.10	0.02	0.00	0.00	0.05	0.00	0.04	0.00
	Overall		345	141		0.21	0.03	0.00	0.01	0.08	0.01	0.03	0.00
Mar	02 March 2022	130	39	30	Postfrontal, high pressure	0.27	0.08	0.00	0.01	0.17	0.00	0.02	0.00
	03 March 2022	131, 132	71	53	Weak prefrontal	0.74	0.12	0.00	0.03	0.26	0.03	0.04	0.00
	04 March 2022	133, 134	42	29	Cold high pressure	1.64	0.02	0.00	0.06	0.05	0.06	0.01	0.00
	13 March 2022	138	8	2	Postfrontal, CAO conditions	0.00	0.11	0.00	0.00	0.59	0.00	0.08	0.00
	14 March 2022	139, 140	38	32	Late postfrontal, cold high pressure; smoke plume sampled from a woodland fire	0.08	0.03	0.00	0.00	0.05	0.00	0.04	0.01
	18 March 2022	141	14	12	Weak postfrontal	0.12	0.02	0.00	0.00	0.03	0.00	0.03	0.07
	26 March 2022	144, 145	29	15	Postfrontal; sampled dust, smoke, and potentially pollen	0.02	0.02	0.00	0.00	0.05	0.00	0.04	0.01
	28 March 2022	146	17	10	Postfrontal	0.02	0.03	0.00	0.00	0.05	0.00	0.05	0.00

	29 March 2022	147, 148	19	4	Postfrontal, high pressure, CAO conditions	0.09	0.08	0.00	0.00	0.16	0.00	0.05	0.02
	Overall		277	187		0.22	0.05	0.00	0.01	0.12	0.01	0.03	0.00
May	03 May 2022	149	15	10	Weak prefrontal; presence of smoke potentially from New Mexico	0.37	0.08	0.00	0.01	0.14	0.01	0.05	0.00
	05 May 2022	150, 151	18	9	Postfrontal	0.03	0.02	0.00	0.00	0.04	0.00	0.02	0.00
	16 May 2022	153, 154	39	5	Prefrontal to an approaching cold front yet also postfrontal to a departing band of precipitation	0.12	0.16	0.00	0.00	0.31	0.00	0.03	0.00
	17 May 2022	155	37	2	Postfrontal	0.06	0.00	0.00	0.00	0.01	0.00	0.01	0.00
	20 May 2022	158	28	19	Warm high pressure, southerly flow due to Bermuda high ² ; haze with potential sampling of bioaerosol	2.19	0.01	0.00	0.08	0.06	0.05	0.00	0.00
	Overall		137	45		0.39	0.02	0.00	0.01	0.08	0.01	0.01	0.00
Mar transit	22 March 2022	142, 143	48	47	High pressure, two days after a cold front and two days before another cold front	0.74	0.04	0.00	0.03	0.10	0.01	0.06	0.00
May transit	18 May 2022	156, 157	67	23	Postfrontal along East Coast, aircraft passed across the cold front on the way to Bermuda	1.10	0.00	0.00	0.04	0.01	0.02	0.00	0.00
	21 May 2022	159, 160	42	14	Warm high pressure, anticyclonic flow around Bermuda high	1.14	0.00	0.00	0.04	0.01	0.03	0.00	0.00
	31 May 2022	161	11	1	Postfrontal	0.18	0.01	0.01	0.01	0.02	0.01	0.02	0.20
	Overall		120	38		1.07	0.00	0.00	0.04	0.01	0.02	0.00	0.00
Jun Bermuda	02 June 2022	162, 163	4	1	Prefrontal	0.83	0.00	0.00	0.03	0.00	0.03	0.00	0.13
	03 June 2022	164	1	0	Prefrontal, tropical system approaching from the southwest	NaN							
	05 June 2022	165	29	24	Could only fly in the morning due to approaching tropical cyclone	1.97	0.00	0.00	0.07	0.00	0.06	0.00	0.00

	07 June 2022	167	1	0	(TC), TC departs 06 June 2022. High behind departing TC	NaN							
	08 June 2022	168, 169	2	1	High pressure behind TC, African dust known to be in domain	5.56	0.47	0.09	0.21	0.86	0.20	0.86	1.97
	10 June 2022	170	1	1	High pressure, isolated thunderstorms, African dust known to be in domain	2.28	0.00	0.00	0.06	0.00	0.01	0.00	0.00
	11 June 2022	172, 173	20	7	High pressure, African dust known to be in domain	0.78	0.10	0.00	0.03	0.20	0.02	0.02	0.00
	13 June 2022	174	25	17	High pressure, African dust known to be in domain but sampled away from dust for contrast	1.31	0.00	0.00	0.05	0.00	0.04	0.00	0.00
	Overall		83	51		1.38	0.00	0.00	0.05	0.01	0.04	0.00	0.00

143 ¹Davis et al. (1997)

144 **Table S9.** Same as Table S8, except forest fire burning of pinion and juniper trees is considered
 145 as the only combustion process contributing to $\text{Na}^+_{\text{comb}}$ and K^+_{comb} .

Category	Date	RF(s)	N PILS samples	N samples w/ derived species	Meteorological conditions and/or relevant notes	Median ss Na^+ ($\mu\text{g m}^{-3}$)	Median $\text{Na}^+_{\text{dust}}$ ($\mu\text{g m}^{-3}$)	Median $\text{Na}^+_{\text{comb}}$ ($\mu\text{g m}^{-3}$)	Median ss Ca^{2+} ($\mu\text{g m}^{-3}$)	Median $\text{Ca}^{2+}_{\text{dust}}$ ($\mu\text{g m}^{-3}$)	Median ss K^+ ($\mu\text{g m}^{-3}$)	Median K^+_{dust} ($\mu\text{g m}^{-3}$)	Median K^+_{comb} ($\mu\text{g m}^{-3}$)
Dec-Feb	30 November 2021	94	7	1	Remains of post-frontal conditions	0.00	0.16	0.00	0.00	0.41	0.00	0.06	0.00
	01 December 2021	95	16	14	Prefrontal, high pressure; smoke in boundary layer near coast	0.11	0.21	0.00	0.00	0.48	0.00	0.05	0.00
	07 December 2021	96	5	3	Postfrontal, cold high pressure behind a strong cold front	0.09	0.10	0.00	0.00	0.22	0.00	0.03	0.00
	11 January 2022	100, 101	6	3	Cold high pressure, cold air outbreak (CAO) conditions	0.34	0.03	0.00	0.01	0.08	0.01	0.01	0.00
	12 January 2022	102, 103	33	11	Cold high pressure	0.16	0.04	0.00	0.01	0.08	0.00	0.02	0.00
	15 January 2022	104	3	2	Postfrontal	0.67	0.02	0.00	0.01	0.04	0.01	0.00	0.00
	18 January 2022	105	11	0	Low pressure moves offshore, sets up CAO conditions	NaN	NaN	NaN	NaN	NaN	NaN	NaN	NaN
	19 January 2022	107, 108	26	6	Short-lived high pressure	0.27	0.04	0.01	0.01	0.07	0.01	0.05	0.06
	24 January 2022	109, 110	26	9	Postfrontal, weak high pressure	0.19	0.04	0.00	0.00	0.07	0.01	0.05	0.02
	26 January 2022	111, 112	20	7	Postfrontal	0.32	0.02	0.04	0.01	0.04	0.01	0.03	0.35
	27 January 2022	113, 114	18	4	Cold high pressure	0.28	0.00	0.00	0.01	0.00	0.01	0.00	0.00
	01 February 2022	115	8	4	High pressure	1.09	0.01	0.00	0.02	0.03	0.02	0.00	0.00
	02 February 2022	116	17	4	High pressure	0.74	0.00	0.00	0.02	0.01	0.03	0.00	0.02

	03 February 2022	117, 118	15	4	High pressure	1.16	0.00	0.00	0.03	0.00	0.04	0.00	0.01
	15 February 2022	120, 121	34	7	Postfrontal conditions, cold high pressure	0.15	0.04	0.00	0.01	0.13	0.01	0.02	0.00
	16 February 2022	122, 123	21	10	Cold high pressure	0.14	0.05	0.00	0.01	0.12	0.00	0.04	0.00
	19 February 2022	124, 125	38	18	Weak postfrontal	0.06	0.02	0.00	0.00	0.11	0.00	0.04	0.00
	22 February 2022	126, 127	25	20	Prefrontal, high pressure	1.69	0.03	0.00	0.04	0.07	0.04	0.00	0.00
	26 February 2022	128, 129	16	14	Postfrontal	0.10	0.02	0.00	0.00	0.05	0.00	0.04	0.00
	Overall		345	141		0.21	0.03	0.00	0.01	0.08	0.01	0.03	0.00
Mar	02 March 2022	130	39	30	Postfrontal, high pressure	0.27	0.07	0.00	0.01	0.17	0.00	0.02	0.00
	03 March 2022	131, 132	71	53	Weak prefrontal	0.76	0.11	0.00	0.03	0.26	0.03	0.04	0.00
	04 March 2022	133, 134	42	29	Cold high pressure	1.65	0.01	0.00	0.06	0.05	0.06	0.01	0.00
	13 March 2022	138	8	2	Postfrontal, CAO conditions	0.00	0.11	0.00	0.00	0.59	0.00	0.08	0.00
	14 March 2022	139, 140	38	32	Late postfrontal, cold high pressure; smoke plume sampled from a woodland fire	0.08	0.03	0.00	0.00	0.05	0.00	0.04	0.01
	18 March 2022	141	14	12	Weak postfrontal	0.12	0.02	0.01	0.00	0.03	0.00	0.03	0.07
	26 March 2022	144, 145	29	15	Postfrontal; sampled dust, smoke, and potentially pollen	0.02	0.02	0.00	0.00	0.05	0.00	0.04	0.01
	28 March 2022	146	17	10	Postfrontal	0.01	0.03	0.00	0.00	0.05	0.00	0.05	0.00
	29 March 2022	147, 148	19	4	Postfrontal, high pressure, CAO conditions	0.09	0.08	0.00	0.00	0.16	0.00	0.05	0.02
	Overall		277	187		0.23	0.05	0.00	0.01	0.12	0.01	0.03	0.00
May	03 May 2022	149	15	10	Weak prefrontal; presence of smoke potentially from New Mexico	0.38	0.07	0.00	0.01	0.14	0.01	0.05	0.00

	05 May 2022	150, 151	18	9	Postfrontal	0.03	0.02	0.00	0.00	0.04	0.00	0.02	0.00
	16 May 2022	153, 154	39	5	Prefrontal to an approaching cold front yet also postfrontal to a departing band of precipitation	0.13	0.15	0.00	0.00	0.31	0.00	0.03	0.00
	17 May 2022	155	37	2	Postfrontal	0.06	0.00	0.00	0.00	0.01	0.00	0.01	0.00
	20 May 2022	158	28	19	Warm high pressure, southerly flow due to Bermuda high ² ; haze with potential sampling of bioaerosol	2.21	0.00	0.00	0.08	0.06	0.06	0.00	0.00
	Overall		137	45		0.41	0.02	0.00	0.01	0.08	0.01	0.01	0.00
Mar transit	22 March 2022	142, 143	48	47	High pressure, two days after a cold front and two days before another cold front	0.75	0.04	0.00	0.03	0.10	0.01	0.06	0.00
	18 May 2022	156, 157	67	23	Postfrontal along East Coast, aircraft passed across the cold front on the way to Bermuda	1.11	0.00	0.00	0.04	0.01	0.02	0.00	0.00
May transit	21 May 2022	159, 160	42	14	Warm high pressure, anticyclonic flow around Bermuda high	1.14	0.00	0.00	0.04	0.01	0.03	0.00	0.00
	31 May 2022	161	11	1	Postfrontal	0.17	0.01	0.02	0.01	0.02	0.01	0.02	0.20
	Overall		120	38		1.08	0.00	0.00	0.04	0.01	0.02	0.00	0.00
	02 June 2022	162, 163	4	1	Prefrontal	0.82	0.00	0.01	0.03	0.00	0.03	0.00	0.13
	03 June 2022	164	1	0	Prefrontal, tropical system approaching from the southwest	NaN							
Jun Bermuda	05 June 2022	165	29	24	Could only fly in the morning due to approaching tropical cyclone (TC). TC departs 06 June 2022.	1.97	0.00	0.00	0.07	0.00	0.06	0.00	0.00
	07 June 2022	167	1	0	High behind departing TC	NaN							
	08 June 2022	168, 169	2	1	High pressure behind TC, African dust known to be in domain	5.47	0.45	0.20	0.21	0.87	0.20	0.87	1.97

	10 June 2022	170	1	1	High pressure, isolated thunderstorms, African dust known to be in domain	2.28	0.00	0.00	0.06	0.00	0.01	0.00	0.00
	11 June 2022	172, 173	20	7	High pressure, African dust known to be in domain	0.80	0.09	0.00	0.03	0.20	0.02	0.01	0.00
	13 June 2022	174	25	17	High pressure, African dust known to be in domain but sampled away from dust for contrast	1.32	0.00	0.00	0.05	0.00	0.04	0.00	0.00
	Overall		83	51		1.38	0.00	0.00	0.05	0.01	0.04	0.00	0.00

146

¹Davis et al. (1997)

147 **Table S10.** Same as Table S8, except industrial operations (i.e., those at steel mills and cement
 148 plants) are considered as the only combustion process contributing to $\text{Na}^+_{\text{comb}}$ and K^+_{comb} .

Category	Date	RF(s)	N PILS samples	N samples w/ derived species	Meteorological conditions and/or relevant notes	Median ss Na^+ ($\mu\text{g m}^{-3}$)	Median $\text{Na}^+_{\text{dust}}$ ($\mu\text{g m}^{-3}$)	Median $\text{Na}^+_{\text{comb}}$ ($\mu\text{g m}^{-3}$)	Median ss Ca^{2+} ($\mu\text{g m}^{-3}$)	Median $\text{Ca}^{2+}_{\text{dust}}$ ($\mu\text{g m}^{-3}$)	Median ss K^+ ($\mu\text{g m}^{-3}$)	Median K^+_{dust} ($\mu\text{g m}^{-3}$)	Median K^+_{comb} ($\mu\text{g m}^{-3}$)
Dec-Feb	30 November 2021	94	7	1	Remains of post-frontal conditions	0.01	0.14	0.00	0.00	0.41	0.00	0.06	0.00
	01 December 2021	95	16	14	Prefrontal, high pressure; smoke in boundary layer near coast	0.18	0.16	0.00	0.01	0.48	0.01	0.05	0.00
	07 December 2021	96	5	3	Postfrontal, cold high pressure behind a strong cold front	0.12	0.07	0.00	0.00	0.22	0.00	0.02	0.00
	11 January 2022	100, 101	6	3	Cold high pressure, cold air outbreak (CAO) conditions	0.35	0.03	0.00	0.01	0.08	0.01	0.01	0.00
	12 January 2022	102, 103	33	11	Cold high pressure	0.16	0.03	0.00	0.01	0.08	0.00	0.02	0.00
	15 January 2022	104	3	2	Postfrontal	0.68	0.01	0.00	0.01	0.04	0.01	0.00	0.00
	18 January 2022	105	11	0	Low pressure moves offshore, sets up CAO conditions	NaN	NaN	NaN	NaN	NaN	NaN	NaN	NaN
	19 January 2022	107, 108	26	6	Short-lived high pressure	0.26	0.03	0.02	0.01	0.07	0.01	0.05	0.06
	24 January 2022	109, 110	26	9	Postfrontal, weak high pressure	0.22	0.04	0.00	0.00	0.08	0.01	0.05	0.02
	26 January 2022	111, 112	20	7	Postfrontal	0.27	0.01	0.09	0.01	0.04	0.01	0.04	0.35
	27 January 2022	113, 114	18	4	Cold high pressure	0.28	0.00	0.00	0.01	0.00	0.01	0.00	0.00
	01 February 2022	115	8	4	High pressure	1.10	0.00	0.00	0.02	0.03	0.02	0.00	0.00
	02 February 2022	116	17	4	High pressure	0.75	0.00	0.00	0.02	0.01	0.03	0.00	0.02

	03 February 2022	117, 118	15	4	High pressure	1.16	0.00	0.00	0.03	0.00	0.04	0.00	0.01
	15 February 2022	120, 121	34	7	Postfrontal conditions, cold high pressure	0.23	0.04	0.00	0.01	0.13	0.01	0.01	0.00
	16 February 2022	122, 123	21	10	Cold high pressure	0.15	0.04	0.00	0.01	0.12	0.00	0.04	0.00
	19 February 2022	124, 125	38	18	Weak postfrontal	0.06	0.02	0.00	0.00	0.11	0.00	0.04	0.00
	22 February 2022	126, 127	25	20	Prefrontal, high pressure	1.73	0.00	0.00	0.05	0.07	0.04	0.00	0.00
	26 February 2022	128, 129	16	14	Postfrontal	0.09	0.02	0.00	0.00	0.05	0.00	0.04	0.00
	Overall		345	141		0.23	0.02	0.00	0.01	0.08	0.01	0.03	0.00
Mar	02 March 2022	130	39	30	Postfrontal, high pressure	0.29	0.04	0.00	0.01	0.17	0.00	0.02	0.00
	03 March 2022	131, 132	71	53	Weak prefrontal	0.81	0.07	0.00	0.03	0.26	0.03	0.04	0.00
	04 March 2022	133, 134	42	29	Cold high pressure	1.66	0.00	0.00	0.06	0.05	0.06	0.01	0.00
	13 March 2022	138	8	2	Postfrontal, CAO conditions	0.00	0.11	0.00	0.00	0.59	0.00	0.08	0.00
	14 March 2022	139, 140	38	32	Late postfrontal, cold high pressure; smoke plume sampled from a woodland fire	0.09	0.03	0.00	0.00	0.05	0.00	0.04	0.01
	18 March 2022	141	14	12	Weak postfrontal	0.11	0.02	0.02	0.00	0.03	0.00	0.03	0.07
	26 March 2022	144, 145	29	15	Postfrontal; sampled dust, smoke, and potentially pollen	0.02	0.02	0.00	0.00	0.05	0.00	0.04	0.01
	28 March 2022	146	17	10	Postfrontal	0.01	0.03	0.00	0.00	0.05	0.00	0.05	0.00
	29 March 2022	147, 148	19	4	Postfrontal, high pressure, CAO conditions	0.10	0.07	0.01	0.00	0.16	0.00	0.05	0.02
	Overall		277	187		0.22	0.03	0.00	0.01	0.12	0.01	0.03	0.00
May	03 May 2022	149	15	10	Weak prefrontal; presence of smoke potentially from New Mexico	0.41	0.06	0.00	0.01	0.14	0.01	0.05	0.00

	05 May 2022	150, 151	18	9	Postfrontal	0.03	0.02	0.00	0.00	0.04	0.00	0.03	0.00
	16 May 2022	153, 154	39	5	Prefrontal to an approaching cold front yet also postfrontal to a departing band of precipitation	0.16	0.10	0.00	0.01	0.31	0.01	0.03	0.00
	17 May 2022	155	37	2	Postfrontal	0.06	0.00	0.00	0.00	0.01	0.00	0.01	0.00
	20 May 2022	158	28	19	Warm high pressure, southerly flow due to Bermuda high ² ; haze with potential sampling of bioaerosol	2.24	0.00	0.00	0.08	0.06	0.06	0.00	0.00
	Overall		137	45		0.45	0.01	0.00	0.01	0.08	0.01	0.01	0.00
Mar transit	22 March 2022	142, 143	48	47	High pressure, two days after a cold front and two days before another cold front	0.77	0.02	0.00	0.03	0.10	0.01	0.06	0.00
	18 May 2022	156, 157	67	23	Postfrontal along East Coast, aircraft passed across the cold front on the way to Bermuda	1.11	0.00	0.00	0.04	0.01	0.02	0.00	0.00
May transit	21 May 2022	159, 160	42	14	Warm high pressure, anticyclonic flow around Bermuda high	1.14	0.00	0.00	0.04	0.01	0.03	0.00	0.00
	31 May 2022	161	11	1	Postfrontal	0.14	0.01	0.05	0.01	0.02	0.01	0.02	0.20
	Overall		120	38		1.08	0.00	0.00	0.04	0.01	0.02	0.00	0.00
	02 June 2022	162, 163	4	1	Prefrontal	0.81	0.00	0.02	0.03	0.00	0.03	0.00	0.13
	03 June 2022	164	1	0	Prefrontal, tropical system approaching from the southwest	NaN							
Jun Bermuda	05 June 2022	165	29	24	Could only fly in the morning due to approaching tropical cyclone (TC). TC departs 06 June 2022.	1.97	0.00	0.00	0.07	0.00	0.06	0.00	0.00
	07 June 2022	167	1	0	High behind departing TC	NaN							
	08 June 2022	168, 169	2	1	High pressure behind TC, African dust known to be in domain	5.24	0.39	0.48	0.20	0.88	0.19	0.88	1.97

	10 June 2022	170	1	1	High pressure, isolated thunderstorms, African dust known to be in domain	2.28	0.00	0.00	0.06	0.00	0.01	0.00	0.00
	11 June 2022	172, 173	20	7	High pressure, African dust known to be in domain	0.83	0.06	0.00	0.03	0.20	0.02	0.01	0.00
	13 June 2022	174	25	17	High pressure, African dust known to be in domain but sampled away from dust for contrast	1.35	0.00	0.00	0.05	0.00	0.04	0.00	0.00
	Overall		83	51		1.38	0.00	0.00	0.05	0.01	0.04	0.00	0.00

149

¹Davis et al. (1997)

150 **Table S11.** Same as Table S8, except inefficient batch combustion in a sauna stove is considered
 151 as the only combustion process contributing to $\text{Na}^+_{\text{comb}}$ and K^+_{comb} .

Category	Date	RF(s)	N PILS samples	N samples w/ derived species	Meteorological conditions and/or relevant notes	Median ss Na^+ ($\mu\text{g m}^{-3}$)	Median $\text{Na}^+_{\text{dust}}$ ($\mu\text{g m}^{-3}$)	Median $\text{Na}^+_{\text{comb}}$ ($\mu\text{g m}^{-3}$)	Median ss Ca^{2+} ($\mu\text{g m}^{-3}$)	Median $\text{Ca}^{2+}_{\text{dust}}$ ($\mu\text{g m}^{-3}$)	Median ss K^+ ($\mu\text{g m}^{-3}$)	Median K^+_{dust} ($\mu\text{g m}^{-3}$)	Median K^+_{comb} ($\mu\text{g m}^{-3}$)
Dec-Feb	30 November 2021	94	7	1	Remains of post-frontal conditions	0.16	0.00	0.00	0.01	0.40	0.01	0.06	0.00
	01 December 2021	95	16	14	Prefrontal, high pressure; smoke in boundary layer near coast	0.35	0.00	0.00	0.01	0.47	0.01	0.05	0.00
	07 December 2021	96	5	3	Postfrontal, cold high pressure behind a strong cold front	0.19	0.00	0.00	0.01	0.22	0.01	0.02	0.00
	11 January 2022	100, 101	6	3	Cold high pressure, cold air outbreak (CAO) conditions	0.36	0.00	0.00	0.01	0.08	0.01	0.01	0.00
	12 January 2022	102, 103	33	11	Cold high pressure	0.21	0.00	0.00	0.01	0.08	0.00	0.02	0.00
	15 January 2022	104	3	2	Postfrontal	0.69	0.00	0.00	0.01	0.04	0.01	0.00	0.00
	18 January 2022	105	11	0	Low pressure moves offshore, sets up CAO conditions	NaN	NaN	NaN	NaN	NaN	NaN	NaN	NaN
	19 January 2022	107, 108	26	6	Short-lived high pressure	0.22	0.02	0.05	0.01	0.07	0.01	0.06	0.06
	24 January 2022	109, 110	26	9	Postfrontal, weak high pressure	0.07	0.00	0.01	0.00	0.09	0.00	0.05	0.02
	26 January 2022	111, 112	20	7	Postfrontal	0.12	0.00	0.27	0.00	0.04	0.00	0.04	0.35
	27 January 2022	113, 114	18	4	Cold high pressure	0.28	0.00	0.00	0.01	0.00	0.01	0.00	0.00
	01 February 2022	115	8	4	High pressure	1.10	0.00	0.00	0.02	0.03	0.02	0.00	0.00
	02 February 2022	116	17	4	High pressure	0.74	0.00	0.00	0.02	0.01	0.03	0.00	0.02

	03 February 2022	117, 118	15	4	High pressure	1.16	0.00	0.00	0.03	0.00	0.04	0.00	0.01
	15 February 2022	120, 121	34	7	Postfrontal conditions, cold high pressure	0.31	0.00	0.00	0.01	0.13	0.01	0.01	0.00
	16 February 2022	122, 123	21	10	Cold high pressure	0.23	0.00	0.00	0.01	0.12	0.01	0.03	0.00
	19 February 2022	124, 125	38	18	Weak postfrontal	0.08	0.01	0.00	0.00	0.11	0.00	0.04	0.00
	22 February 2022	126, 127	25	20	Prefrontal, high pressure	1.73	0.00	0.00	0.05	0.07	0.04	0.00	0.00
	26 February 2022	128, 129	16	14	Postfrontal	0.10	0.01	0.00	0.00	0.05	0.00	0.04	0.00
	Overall	345	141			0.24	0.00	0.00	0.01	0.08	0.01	0.02	0.00
Mar	02 March 2022	130	39	30	Postfrontal, high pressure	0.31	0.00	0.00	0.01	0.17	0.01	0.01	0.00
	03 March 2022	131, 132	71	53	Weak prefrontal	0.86	0.00	0.00	0.03	0.26	0.03	0.03	0.00
	04 March 2022	133, 134	42	29	Cold high pressure	1.51	0.00	0.00	0.05	0.05	0.05	0.01	0.00
	13 March 2022	138	8	2	Postfrontal, CAO conditions	0.11	0.00	0.00	0.00	0.59	0.00	0.08	0.00
	14 March 2022	139, 140	38	32	Late postfrontal, cold high pressure; smoke plume sampled from a woodland fire	0.08	0.01	0.01	0.00	0.06	0.00	0.04	0.01
	18 March 2022	141	14	12	Weak postfrontal	0.10	0.01	0.05	0.00	0.04	0.00	0.04	0.07
	26 March 2022	144, 145	29	15	Postfrontal; sampled dust, smoke, and potentially pollen	0.03	0.02	0.01	0.00	0.05	0.00	0.04	0.01
	28 March 2022	146	17	10	Postfrontal	0.05	0.00	0.00	0.00	0.05	0.00	0.04	0.00
	29 March 2022	147, 148	19	4	Postfrontal, high pressure, CAO conditions	0.12	0.03	0.02	0.00	0.15	0.00	0.05	0.02
	Overall	277	187			0.25	0.00	0.00	0.01	0.12	0.01	0.03	0.00
May	03 May 2022	149	15	10	Weak prefrontal; presence of smoke potentially from New Mexico	0.43	0.00	0.00	0.01	0.14	0.02	0.05	0.00

	05 May 2022	150, 151	18	9	Postfrontal	0.02	0.00	0.00	0.00	0.05	0.00	0.03	0.00
	16 May 2022	153, 154	39	5	Prefrontal to an approaching cold front yet also postfrontal to a departing band of precipitation	0.26	0.00	0.00	0.01	0.31	0.01	0.02	0.00
	17 May 2022	155	37	2	Postfrontal	0.06	0.00	0.00	0.00	0.01	0.00	0.01	0.00
	20 May 2022	158	28	19	Warm high pressure, southerly flow due to Bermuda high ² ; haze with potential sampling of bioaerosol	2.24	0.00	0.00	0.08	0.06	0.06	0.00	0.00
	Overall		137	45		0.45	0.00	0.00	0.02	0.08	0.01	0.01	0.00
Mar transit	22 March 2022	142, 143	48	47	High pressure, two days after a cold front and two days before another cold front	0.72	0.00	0.00	0.03	0.10	0.02	0.05	0.00
	18 May 2022	156, 157	67	23	Postfrontal along East Coast, aircraft passed across the cold front on the way to Bermuda	1.11	0.00	0.00	0.04	0.01	0.02	0.00	0.00
May transit	21 May 2022	159, 160	42	14	Warm high pressure, anticyclonic flow around Bermuda high	1.14	0.00	0.00	0.04	0.01	0.03	0.00	0.00
	31 May 2022	161	11	1	Postfrontal	0.04	0.01	0.15	0.00	0.02	0.00	0.02	0.20
	Overall		120	38		1.08	0.00	0.00	0.04	0.01	0.02	0.00	0.00
	02 June 2022	162, 163	4	1	Prefrontal	0.77	0.00	0.05	0.03	0.00	0.03	0.00	0.13
	03 June 2022	164	1	0	Prefrontal, tropical system approaching from the southwest	NaN							
Jun Bermuda	05 June 2022	165	29	24	Could only fly in the morning due to approaching tropical cyclone (TC), TC departs 06 June 2022.	1.97	0.00	0.00	0.07	0.00	0.06	0.00	0.00
	07 June 2022	167	1	0	High behind departing TC	NaN							
	08 June 2022	168, 169	2	1	High pressure behind TC, African dust known to be in domain	4.37	0.26	1.48	0.17	0.91	0.16	0.91	1.97

	10 June 2022	170	1	1	High pressure, isolated thunderstorms, African dust known to be in domain	2.28	0.00	0.00	0.06	0.00	0.01	0.00	0.00
	11 June 2022	172, 173	20	7	High pressure, African dust known to be in domain	0.89	0.00	0.00	0.03	0.19	0.03	0.01	0.00
	13 June 2022	174	25	17	High pressure, African dust known to be in domain but sampled away from dust for contrast	1.38	0.00	0.00	0.05	0.00	0.04	0.00	0.00
	Overall		83	51		1.42	0.00	0.00	0.05	0.01	0.04	0.00	0.00

152

¹Davis et al. (1997)

153 **Table S12.** Same as Table S8, except fossil fuel combustion by motor vehicles is considered as
 154 the only combustion process contributing to $\text{Na}^+_{\text{comb}}$ and K^+_{comb} .

Category	Date	RF(s)	N PILS samples	N samples w/ derived species	Meteorological conditions and/or relevant notes	Median ss Na^+ ($\mu\text{g m}^{-3}$)	Median $\text{Na}^+_{\text{dust}}$ ($\mu\text{g m}^{-3}$)	Median $\text{Na}^+_{\text{comb}}$ ($\mu\text{g m}^{-3}$)	Median ss Ca^{2+} ($\mu\text{g m}^{-3}$)	Median $\text{Ca}^{2+}_{\text{dust}}$ ($\mu\text{g m}^{-3}$)	Median ss K^+ ($\mu\text{g m}^{-3}$)	Median K^+_{dust} ($\mu\text{g m}^{-3}$)	Median K^+_{comb} ($\mu\text{g m}^{-3}$)
Dec-Feb	30 November 2021	94	7	1	Remains of post-frontal conditions	0.16	0.00	0.00	0.01	0.40	0.01	0.06	0.00
	01 December 2021	95	16	14	Prefrontal, high pressure; smoke in boundary layer near coast	0.35	0.00	0.00	0.01	0.47	0.01	0.05	0.00
	07 December 2021	96	5	3	Postfrontal, cold high pressure behind a strong cold front	0.19	0.00	0.00	0.01	0.22	0.01	0.02	0.00
	11 January 2022	100, 101	6	3	Cold high pressure, cold air outbreak (CAO) conditions	0.36	0.00	0.00	0.01	0.08	0.01	0.01	0.00
	12 January 2022	102, 103	33	11	Cold high pressure	0.21	0.00	0.00	0.01	0.08	0.00	0.02	0.00
	15 January 2022	104	3	2	Postfrontal	0.69	0.00	0.00	0.01	0.04	0.01	0.00	0.00
	18 January 2022	105	11	0	Low pressure moves offshore, sets up CAO conditions	NaN	NaN	NaN	NaN	NaN	NaN	NaN	NaN
	19 January 2022	107, 108	26	6	Short-lived high pressure	0.21	0.01	0.05	0.01	0.07	0.01	0.06	0.06
	24 January 2022	109, 110	26	9	Postfrontal, weak high pressure	0.07	0.00	0.02	0.00	0.09	0.00	0.05	0.02
	26 January 2022	111, 112	20	7	Postfrontal	0.05	0.00	0.32	0.00	0.05	0.00	0.05	0.35
	27 January 2022	113, 114	18	4	Cold high pressure	0.28	0.00	0.00	0.01	0.00	0.01	0.00	0.00
	01 February 2022	115	8	4	High pressure	1.10	0.00	0.00	0.02	0.03	0.02	0.00	0.00
	02 February 2022	116	17	4	High pressure	0.74	0.00	0.00	0.02	0.01	0.03	0.00	0.02

	03 February 2022	117, 118	15	4	High pressure	1.16	0.00	0.00	0.03	0.00	0.04	0.00	0.01
	15 February 2022	120, 121	34	7	Postfrontal conditions, cold high pressure	0.31	0.00	0.00	0.01	0.13	0.01	0.01	0.00
	16 February 2022	122, 123	21	10	Cold high pressure	0.22	0.00	0.00	0.01	0.12	0.01	0.03	0.00
	19 February 2022	124, 125	38	18	Weak postfrontal	0.07	0.00	0.00	0.00	0.11	0.00	0.04	0.00
	22 February 2022	126, 127	25	20	Prefrontal, high pressure	1.73	0.00	0.00	0.05	0.07	0.04	0.00	0.00
	26 February 2022	128, 129	16	14	Postfrontal	0.10	0.00	0.00	0.00	0.05	0.00	0.04	0.00
	Overall	345	141			0.24	0.00	0.00	0.01	0.08	0.01	0.02	0.00
Mar	02 March 2022	130	39	30	Postfrontal, high pressure	0.29	0.00	0.00	0.01	0.17	0.01	0.01	0.00
	03 March 2022	131, 132	71	53	Weak prefrontal	0.86	0.00	0.00	0.03	0.26	0.03	0.03	0.00
	04 March 2022	133, 134	42	29	Cold high pressure	1.51	0.00	0.00	0.05	0.05	0.05	0.01	0.00
	13 March 2022	138	8	2	Postfrontal, CAO conditions	0.11	0.00	0.00	0.00	0.59	0.00	0.08	0.00
	14 March 2022	139, 140	38	32	Late postfrontal, cold high pressure; smoke plume sampled from a woodland fire	0.08	0.00	0.01	0.00	0.06	0.00	0.04	0.01
	18 March 2022	141	14	12	Weak postfrontal	0.08	0.01	0.06	0.00	0.04	0.00	0.04	0.07
	26 March 2022	144, 145	29	15	Postfrontal; sampled dust, smoke, and potentially pollen	0.04	0.02	0.01	0.00	0.05	0.00	0.04	0.01
	28 March 2022	146	17	10	Postfrontal	0.05	0.00	0.00	0.00	0.05	0.00	0.04	0.00
	29 March 2022	147, 148	19	4	Postfrontal, high pressure, CAO conditions	0.13	0.02	0.02	0.00	0.15	0.00	0.05	0.02
	Overall	277	187			0.25	0.00	0.00	0.01	0.12	0.01	0.03	0.00
May	03 May 2022	149	15	10	Weak prefrontal; presence of smoke potentially from New Mexico	0.40	0.00	0.00	0.01	0.14	0.01	0.05	0.00

	05 May 2022	150, 151	18	9	Postfrontal	0.02	0.00	0.00	0.00	0.05	0.00	0.03	0.00
	16 May 2022	153, 154	39	5	Prefrontal to an approaching cold front yet also postfrontal to a departing band of precipitation	0.29	0.00	0.00	0.01	0.31	0.01	0.02	0.00
	17 May 2022	155	37	2	Postfrontal	0.06	0.00	0.00	0.00	0.01	0.00	0.01	0.00
	20 May 2022	158	28	19	Warm high pressure, southerly flow due to Bermuda high ² ; haze with potential sampling of bioaerosol	2.24	0.00	0.00	0.08	0.06	0.06	0.00	0.00
	Overall		137	45		0.42	0.00	0.00	0.01	0.08	0.01	0.01	0.00
Mar transit	22 March 2022	142, 143	48	47	High pressure, two days after a cold front and two days before another cold front	0.72	0.00	0.00	0.03	0.10	0.02	0.05	0.00
	18 May 2022	156, 157	67	23	Postfrontal along East Coast, aircraft passed across the cold front on the way to Bermuda	1.11	0.00	0.00	0.04	0.01	0.02	0.00	0.00
May transit	21 May 2022	159, 160	42	14	Warm high pressure, anticyclonic flow around Bermuda high	1.14	0.00	0.00	0.04	0.01	0.03	0.00	0.00
	31 May 2022	161	11	1	Postfrontal	0.01	0.01	0.18	0.00	0.02	0.00	0.02	0.20
	Overall		120	38		1.08	0.00	0.00	0.04	0.01	0.02	0.00	0.00
	02 June 2022	162, 163	4	1	Prefrontal	0.76	0.00	0.07	0.03	0.00	0.03	0.00	0.13
	03 June 2022	164	1	0	Prefrontal, tropical system approaching from the southwest	NaN							
Jun Bermuda	05 June 2022	165	29	24	Could only fly in the morning due to approaching tropical cyclone (TC), TC departs 06 June 2022.	1.97	0.00	0.00	0.07	0.00	0.06	0.00	0.00
	07 June 2022	167	1	0	High behind departing TC	NaN							
	08 June 2022	168, 169	2	1	High pressure behind TC, African dust known to be in domain	4.09	0.23	1.79	0.16	0.92	0.15	0.92	1.97

	10 June 2022	170	1	1	High pressure, isolated thunderstorms, African dust known to be in domain	2.28	0.00	0.00	0.06	0.00	0.01	0.00	0.00
	11 June 2022	172, 173	20	7	High pressure, African dust known to be in domain	0.89	0.00	0.00	0.03	0.19	0.03	0.01	0.00
	13 June 2022	174	25	17	High pressure, African dust known to be in domain but sampled away from dust for contrast	1.38	0.00	0.00	0.05	0.00	0.04	0.00	0.00
155	Overall	83	51			1.42	0.00	0.00	0.05	0.01	0.04	0.00	0.00

¹Davis et al. (1997)

156 **Table S13.** Same as Table S8, except burning of pulverized western coal comprised of low sulfur
 157 (0.5%) and high ash (22%) at a coal-fired power plant is considered as the only combustion process
 158 contributing to $\text{Na}^+_{\text{comb}}$ and K^+_{comb} .

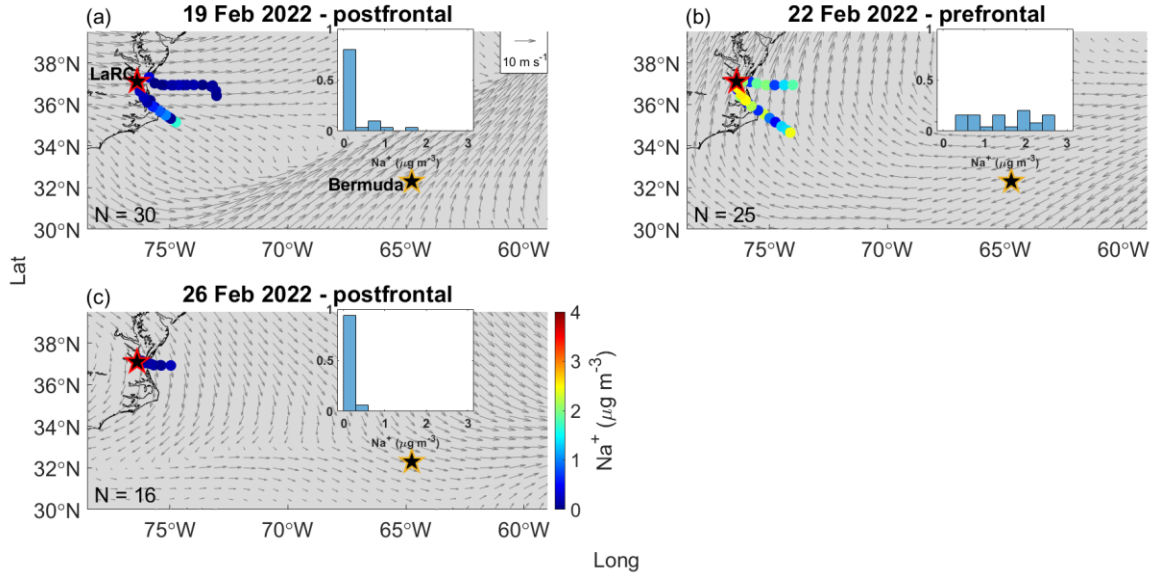
Category	Date	RF(s)	N PILS samples	N samples w/ derived species	Meteorological conditions and/or relevant notes	Median ss Na^+ ($\mu\text{g m}^{-3}$)	Median $\text{Na}^+_{\text{dust}}$ ($\mu\text{g m}^{-3}$)	Median $\text{Na}^+_{\text{comb}}$ ($\mu\text{g m}^{-3}$)	Median ss Ca^{2+} ($\mu\text{g m}^{-3}$)	Median $\text{Ca}^{2+}_{\text{dust}}$ ($\mu\text{g m}^{-3}$)	Median ss K^+ ($\mu\text{g m}^{-3}$)	Median K^+_{dust} ($\mu\text{g m}^{-3}$)	Median K^+_{comb} ($\mu\text{g m}^{-3}$)
Dec-Feb	30 November 2021	94	7	1	Remains of post-frontal conditions	0.16	0.00	0.00	0.01	0.40	0.01	0.06	0.00
	01 December 2021	95	16	14	Prefrontal, high pressure; smoke in boundary layer near coast	0.35	0.00	0.00	0.01	0.47	0.01	0.05	0.00
	07 December 2021	96	5	3	Postfrontal, cold high pressure behind a strong cold front	0.19	0.00	0.00	0.01	0.22	0.01	0.02	0.00
	11 January 2022	100, 101	6	3	Cold high pressure, cold air outbreak (CAO) conditions	0.36	0.00	0.00	0.01	0.08	0.01	0.01	0.00
	12 January 2022	102, 103	33	11	Cold high pressure	0.16	0.00	0.00	0.01	0.08	0.00	0.03	0.00
	15 January 2022	104	3	2	Postfrontal	0.69	0.00	0.00	0.01	0.04	0.01	0.00	0.00
	18 January 2022	105	11	0	Low pressure moves offshore, sets up CAO conditions	NaN	NaN	NaN	NaN	NaN	NaN	NaN	NaN
	19 January 2022	107, 108	26	6	Short-lived high pressure	0.00	0.01	0.19	0.00	0.07	0.00	0.06	0.06
	24 January 2022	109, 110	26	9	Postfrontal, weak high pressure	0.07	0.00	0.06	0.00	0.09	0.00	0.05	0.02
	26 January 2022	111, 112	20	7	Postfrontal	0.00	0.00	0.37	0.00	0.05	0.00	0.05	0.35
	27 January 2022	113, 114	18	4	Cold high pressure	0.28	0.00	0.00	0.01	0.00	0.01	0.00	0.00
	01 February 2022	115	8	4	High pressure	1.10	0.00	0.00	0.02	0.03	0.02	0.00	0.00
	02 February 2022	116	17	4	High pressure	0.72	0.00	0.00	0.02	0.01	0.02	0.00	0.02

	03 February 2022	117, 118	15	4	High pressure	1.16	0.00	0.00	0.03	0.00	0.04	0.00	0.01
	15 February 2022	120, 121	34	7	Postfrontal conditions, cold high pressure	0.31	0.00	0.00	0.01	0.13	0.01	0.01	0.00
	16 February 2022	122, 123	21	10	Cold high pressure	0.16	0.00	0.00	0.01	0.12	0.00	0.03	0.00
	19 February 2022	124, 125	38	18	Weak postfrontal	0.04	0.00	0.00	0.00	0.11	0.00	0.04	0.00
	22 February 2022	126, 127	25	20	Prefrontal, high pressure	1.73	0.00	0.00	0.05	0.07	0.04	0.00	0.00
	26 February 2022	128, 129	16	14	Postfrontal	0.08	0.00	0.00	0.00	0.05	0.00	0.04	0.00
	Overall	345	141			0.20	0.00	0.00	0.01	0.08	0.01	0.03	0.00
Mar	02 March 2022	130	39	30	Postfrontal, high pressure	0.22	0.00	0.00	0.01	0.17	0.00	0.01	0.00
	03 March 2022	131, 132	71	53	Weak prefrontal	0.83	0.00	0.00	0.03	0.26	0.03	0.03	0.00
	04 March 2022	133, 134	42	29	Cold high pressure	1.51	0.00	0.00	0.06	0.05	0.05	0.01	0.00
	13 March 2022	138	8	2	Postfrontal, CAO conditions	0.11	0.00	0.00	0.00	0.59	0.00	0.08	0.00
	14 March 2022	139, 140	38	32	Late postfrontal, cold high pressure; smoke plume sampled from a woodland fire	0.06	0.00	0.01	0.00	0.06	0.00	0.04	0.01
	18 March 2022	141	14	12	Weak postfrontal	0.00	0.00	0.12	0.00	0.04	0.00	0.04	0.07
	26 March 2022	144, 145	29	15	Postfrontal; sampled dust, smoke, and potentially pollen	0.02	0.00	0.01	0.00	0.05	0.00	0.04	0.01
	28 March 2022	146	17	10	Postfrontal	0.07	0.00	0.00	0.00	0.06	0.00	0.04	0.00
	29 March 2022	147, 148	19	4	Postfrontal, high pressure, CAO conditions	0.13	0.00	0.04	0.00	0.15	0.00	0.05	0.02
	Overall	277	187			0.18	0.00	0.00	0.01	0.12	0.01	0.03	0.00
May	03 May 2022	149	15	10	Weak prefrontal; presence of smoke potentially from New Mexico	0.39	0.00	0.00	0.01	0.14	0.01	0.05	0.00

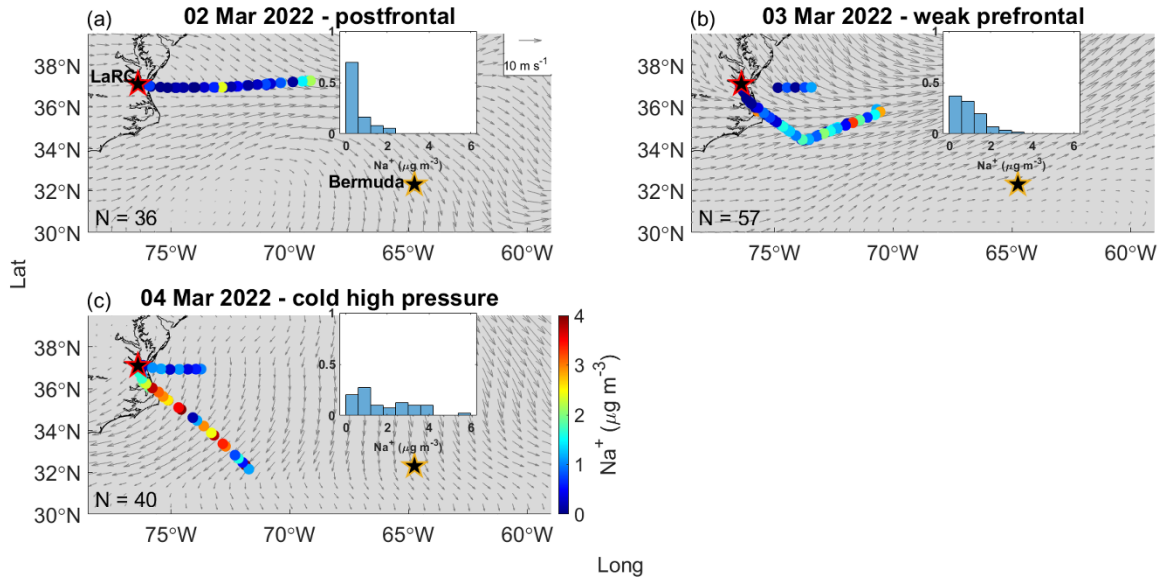
	05 May 2022	150, 151	18	9	Postfrontal	0.02	0.00	0.00	0.00	0.05	0.00	0.03	0.00
	16 May 2022	153, 154	39	5	Prefrontal to an approaching cold front yet also postfrontal to a departing band of precipitation	0.29	0.00	0.00	0.01	0.31	0.01	0.02	0.00
	17 May 2022	155	37	2	Postfrontal	0.06	0.00	0.00	0.00	0.01	0.00	0.01	0.00
	20 May 2022	158	28	19	Warm high pressure, southerly flow due to Bermuda high ² ; haze with potential sampling of bioaerosol	2.24	0.00	0.00	0.08	0.06	0.06	0.00	0.00
	Overall		137	45		0.42	0.00	0.00	0.01	0.08	0.01	0.01	0.00
Mar transit	22 March 2022	142, 143	48	47	High pressure, two days after a cold front and two days before another cold front	0.45	0.00	0.00	0.02	0.10	0.01	0.05	0.00
	18 May 2022	156, 157	67	23	Postfrontal along East Coast, aircraft passed across the cold front on the way to Bermuda	1.11	0.00	0.00	0.04	0.01	0.02	0.00	0.00
May transit	21 May 2022	159, 160	42	14	Warm high pressure, anticyclonic flow around Bermuda high	1.14	0.00	0.00	0.04	0.01	0.03	0.00	0.00
	31 May 2022	161	11	1	Postfrontal	0.00	0.00	0.20	0.00	0.02	0.00	0.02	0.20
	Overall		120	38		1.08	0.00	0.00	0.04	0.01	0.02	0.00	0.00
	02 June 2022	162, 163	4	1	Prefrontal	0.56	0.00	0.27	0.02	0.01	0.02	0.01	0.13
	03 June 2022	164	1	0	Prefrontal, tropical system approaching from the southwest	NaN							
Jun Bermuda	05 June 2022	165	29	24	Could only fly in the morning due to approaching tropical cyclone (TC), TC departs 06 June 2022.	1.94	0.00	0.00	0.07	0.00	0.06	0.00	0.00
	07 June 2022	167	1	0	High behind departing TC	NaN							
	08 June 2022	168, 169	2	1	High pressure behind TC, African dust known to be in domain	0.00	0.18	5.94	0.00	1.07	0.00	1.08	1.96

	10 June 2022	170	1	1	High pressure, isolated thunderstorms, African dust known to be in domain	2.28	0.00	0.00	0.06	0.00	0.01	0.00	0.00
	11 June 2022	172, 173	20	7	High pressure, African dust known to be in domain	0.89	0.00	0.00	0.03	0.19	0.03	0.01	0.00
	13 June 2022	174	25	17	High pressure, African dust known to be in domain but sampled away from dust for contrast	1.38	0.00	0.00	0.05	0.00	0.04	0.00	0.00
159	Overall	83	51			1.34	0.00	0.00	0.05	0.01	0.04	0.00	0.00

¹Davis et al. (1997)

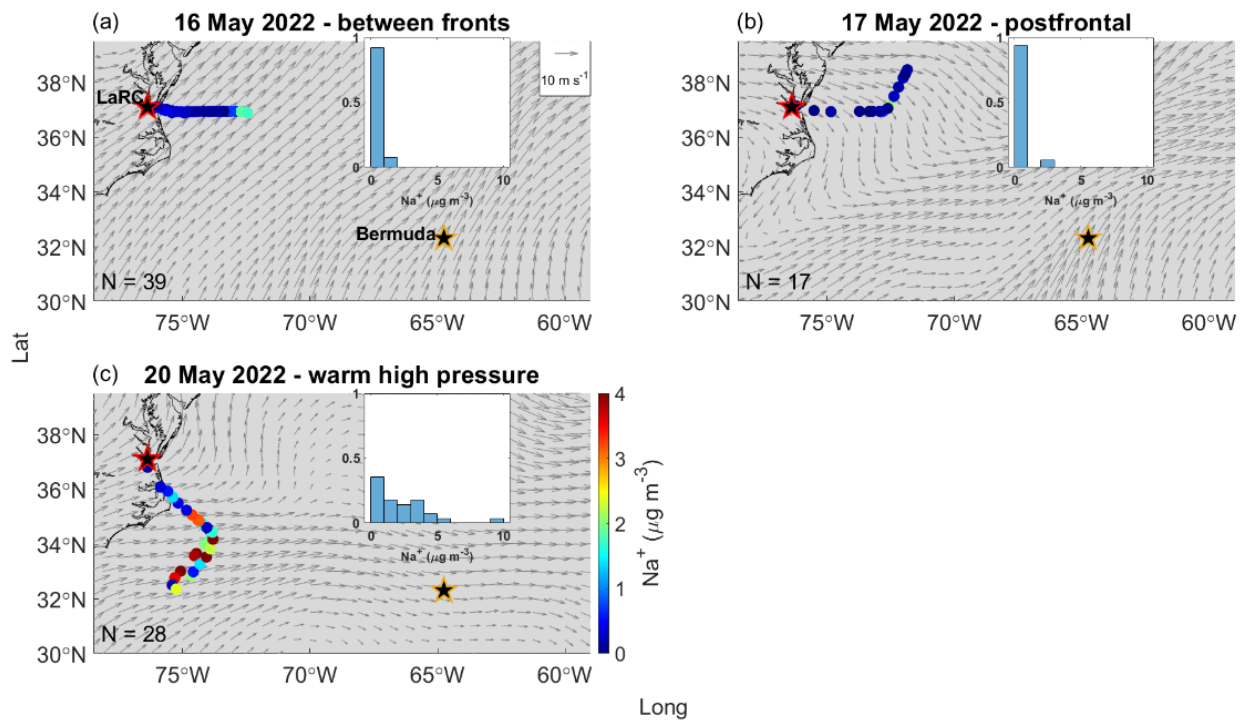


160
161 **Figure S1.** Bulk PILS Na^+ mass concentrations from clear ensembles during flights experiencing
162 (a) postfrontal conditions on 19 February 2022 (RFs 124 and 125) (b) prefrontal conditions on
163 22 February 2022 (RFs 126 and 127), and (c) postfrontal conditions on 26 February 2022 (RFs
164 128 and 129). NASA Langley Research Center (LaRC) and Bermuda are marked with red-edged
165 and gold-edged stars, respectively. Normalized histograms in each panel show the distribution of
166 bulk PILS Na^+ mass concentrations for the date indicated since overlap among the colored dots
167 can hide some from view. Grey arrows in each panel indicate the average magnitude and
168 direction of winds at 950 hPa from MERRA-2 at 3-hour time resolution during periods relevant
169 to each RF.



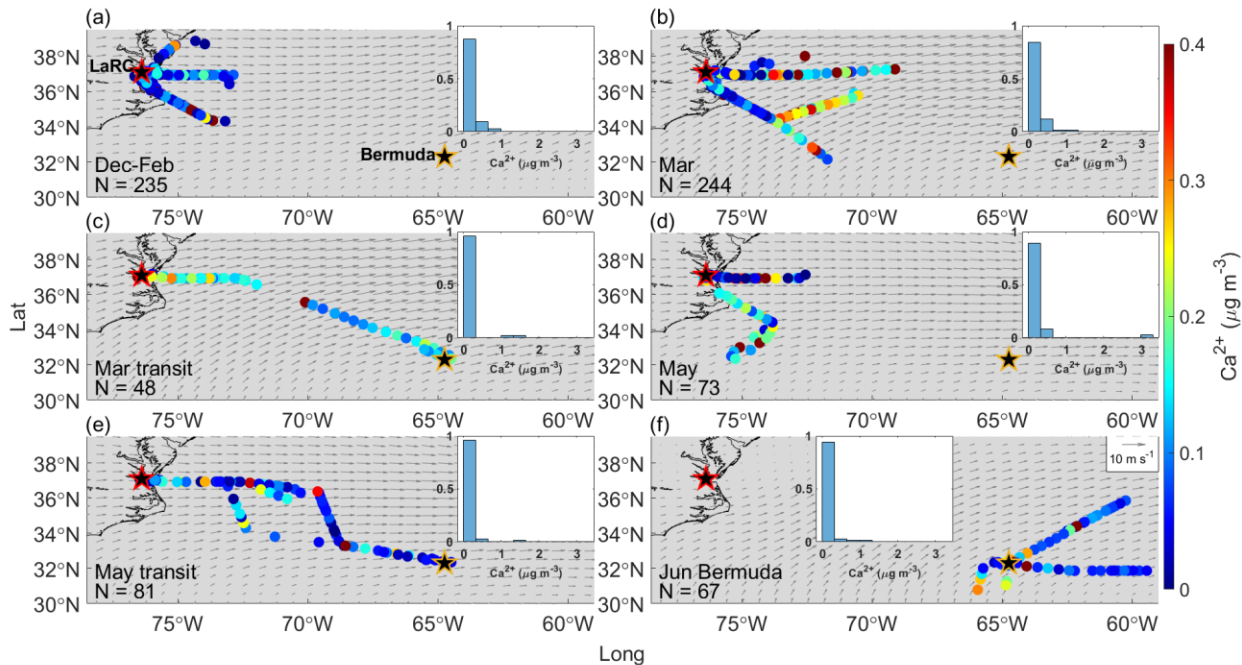
170

171 **Figure S2.** Same as Fig. S1 except for (a) postfrontal conditions on 02 March 2022 (RF 130), (b)
 172 weak prefrontal conditions on 03 March 2022 (RFs 131 and 132), and (c) cold high pressure on
 173 04 March 2022 (RFs 133 and 134).



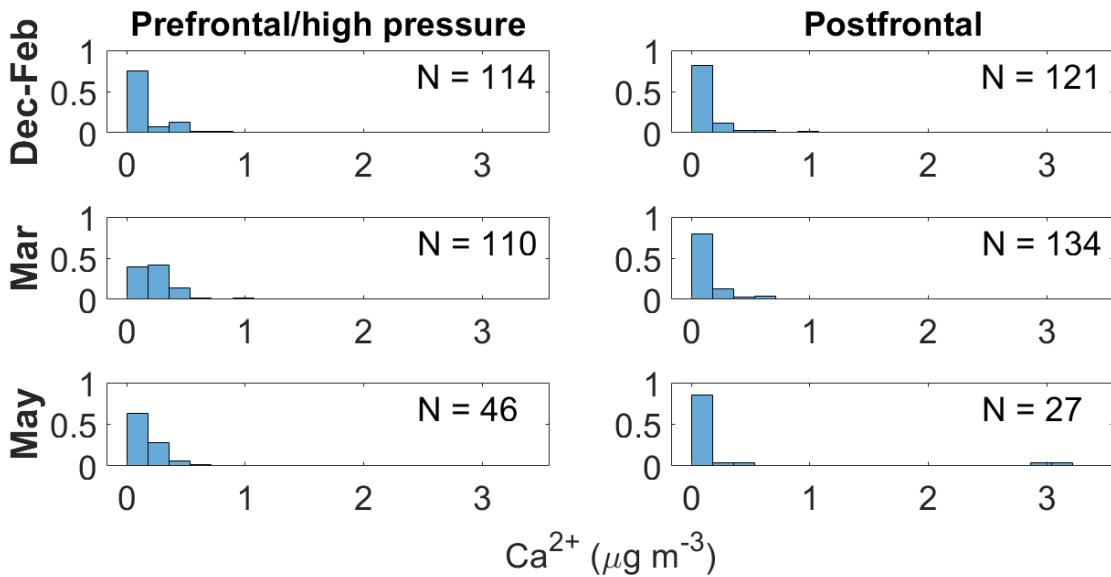
174

175 **Figure S3.** Same as Fig. S1 except for (a) conditions between fronts on 16 May 2022 (RFs 153
 176 and 154), (b) postfrontal conditions on 17 May 2022 (RF 155), and (c) warm high pressure on 20
 177 May 2022 (RF 158).



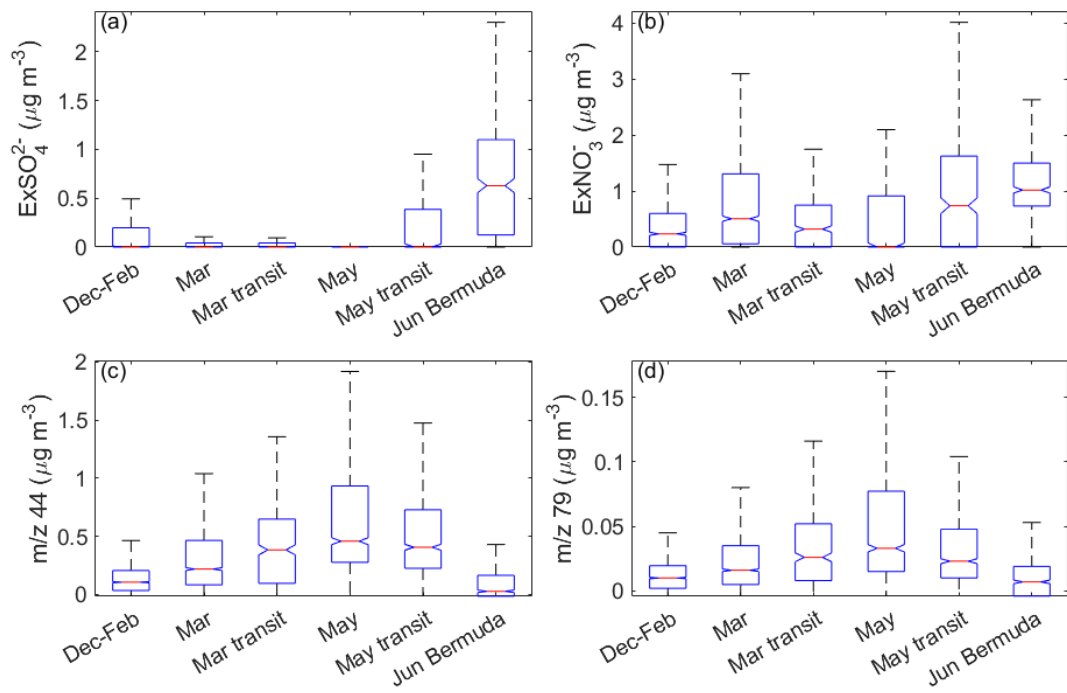
178

179 **Figure S4.** Bulk PILS Ca^{2+} mass concentrations from clear ensembles during (a) December
 180 2021–February 2022, (b) March 2022, (c) March 2022 transit flights between LaRC (marked
 181 with a red-edged star) and Bermuda (marked with a golden-edged star), (d) May 2022,
 182 (e) May 2022 transit flights between LaRC and Bermuda, and (f) the Bermuda field campaign in June
 183 2022. Normalized histograms in each panel show the distribution of bulk PILS Ca^{2+} mass
 184 concentrations for that specific category since overlap among the colored dots can hide some
 185 from view. Grey arrows indicate the average magnitude and direction of MERRA-2 winds at 950
 186 hPa for the month(s) relevant to each category.



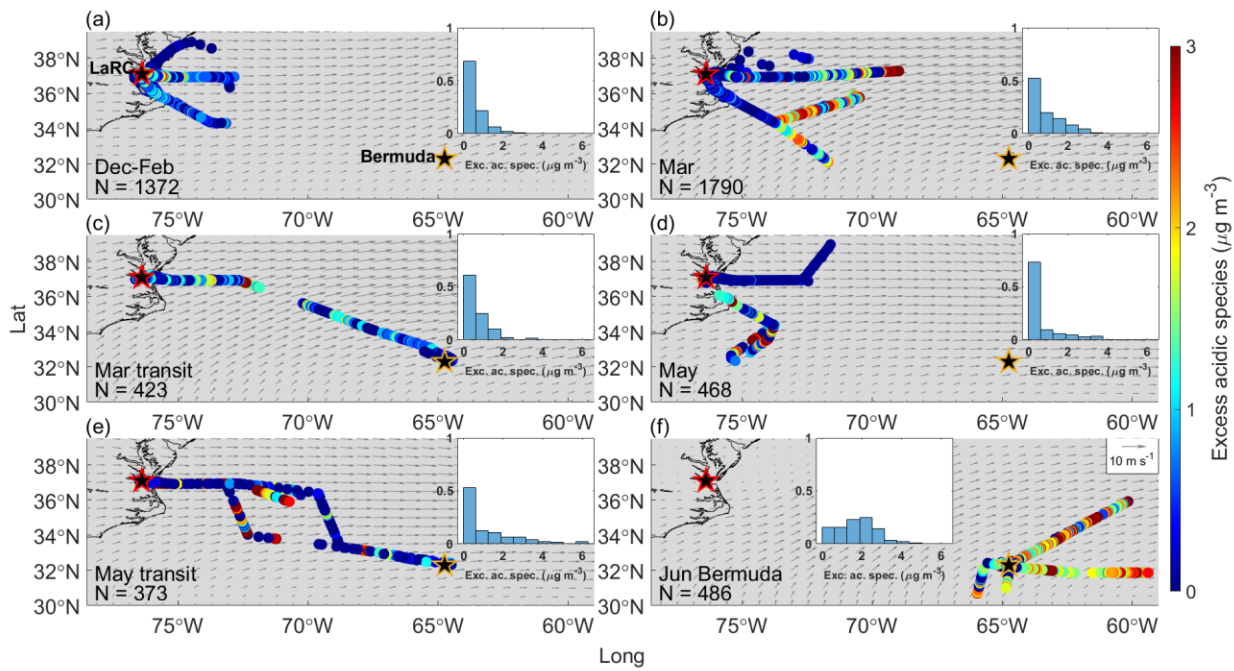
187

188 **Figure S5.** Normalized histograms showing differences in bulk PILS Ca^{2+} mass concentration
 189 from clear ensembles occurring in prefrontal and/or high-pressure versus postfrontal conditions
 190 for December–February (top row), March (middle row), and May (bottom row). These categories
 191 are shown as they represent flights occurring in and around the East Coast, eliminating coastal
 192 versus open-ocean sampling as a confounding variable.



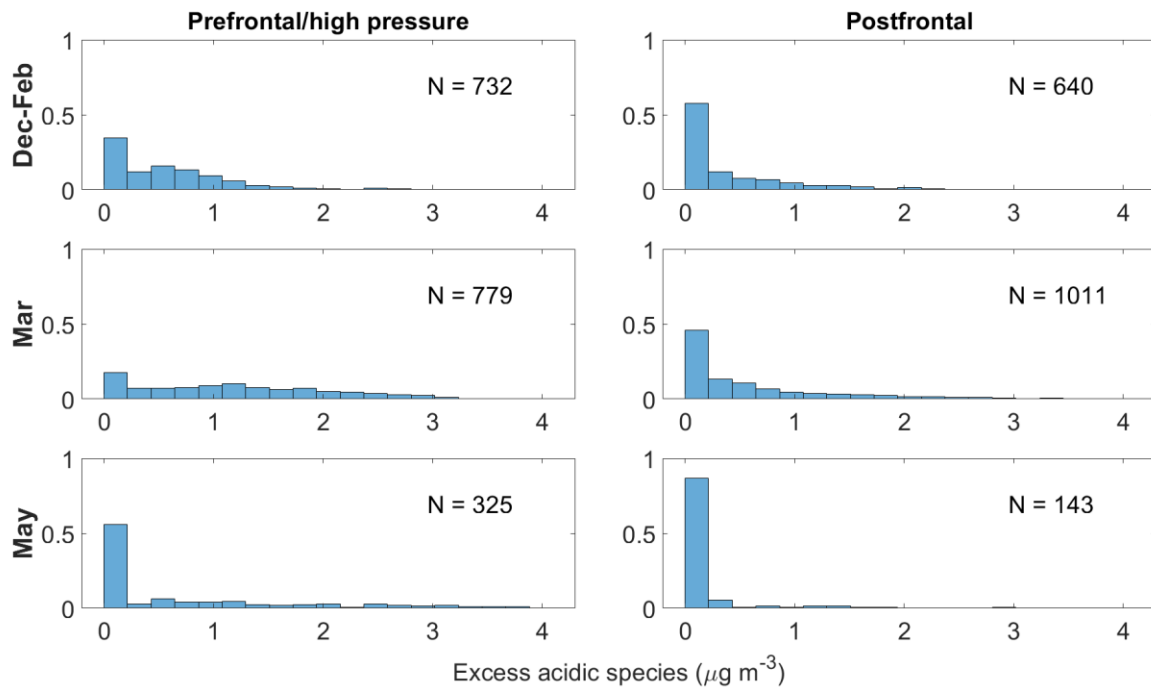
193

194 **Figure S6.** Notched box plots showing seasonal/categories differences in mass concentrations
 195 from clear ensembles of (a) excess SO₄²⁻ (ExSO₄²⁻), (b) excess NO₃⁻ (ExNO₃⁻), and spectral
 196 markers for (c) oxygenated organics, *m/z* 44, and (d) methanesulfonic acid (MSA), *m/z* 79.

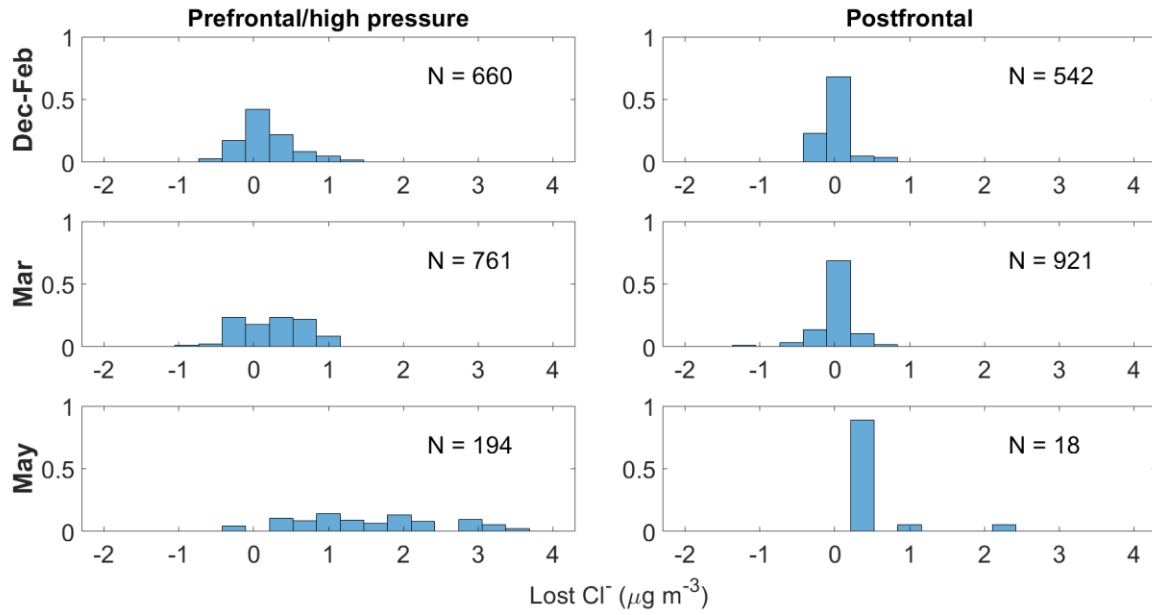


197

198 **Figure S7.** Same as Fig. S4, except for derived mass concentrations of excess acidic species.

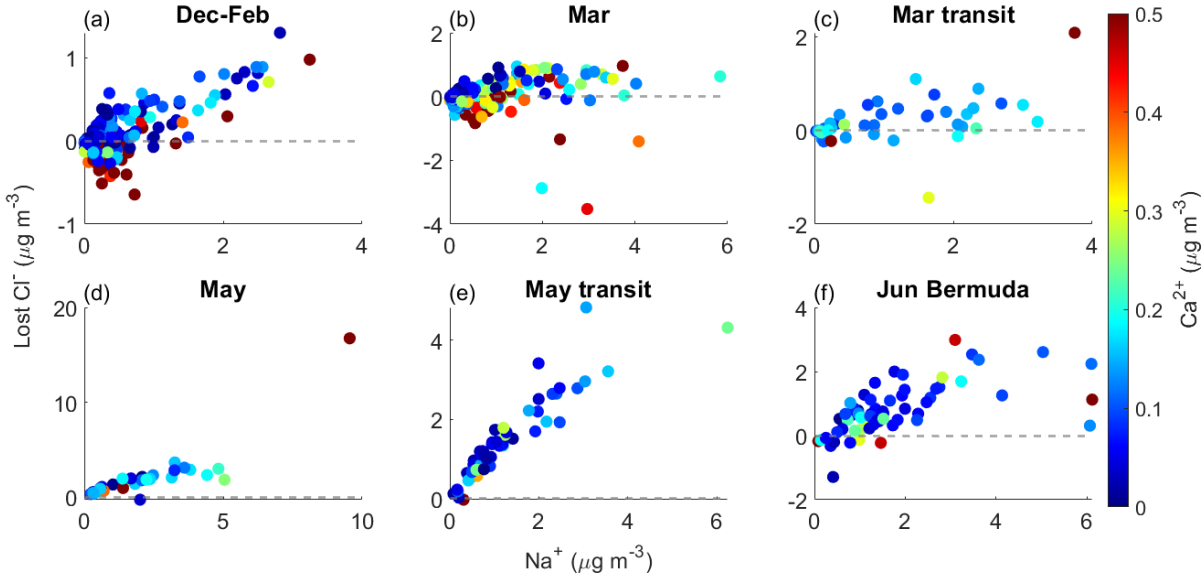


200 **Figure S8.** Same as Fig. S5, except for mass concentrations of excess acidic species.



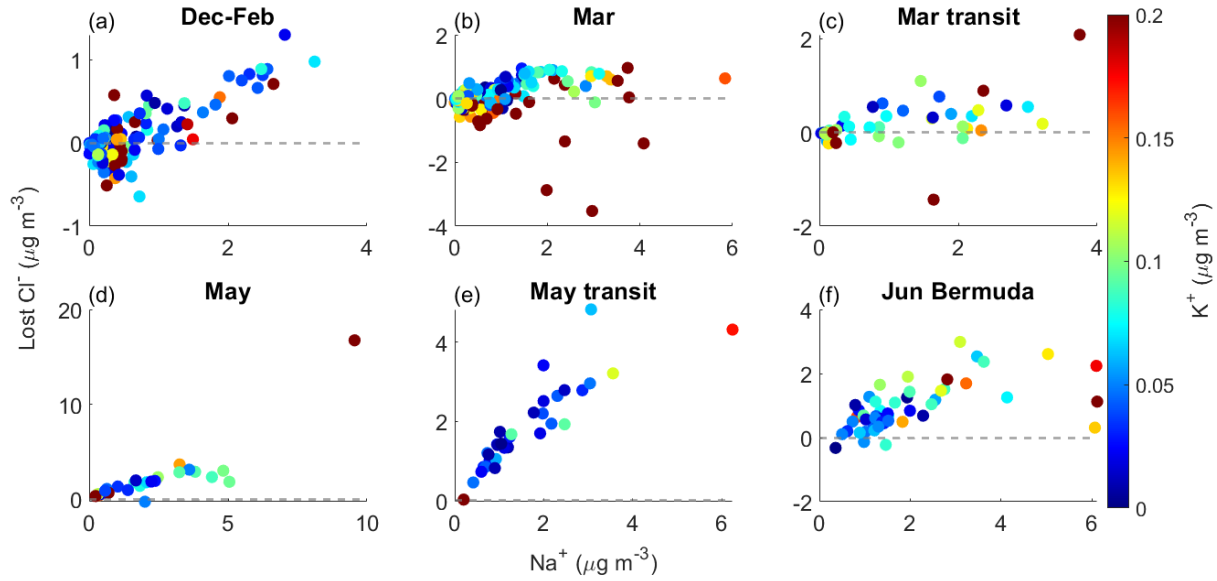
201

202 **Figure S9.** Same as Fig. S5, except for lost Cl^- mass concentration.



203

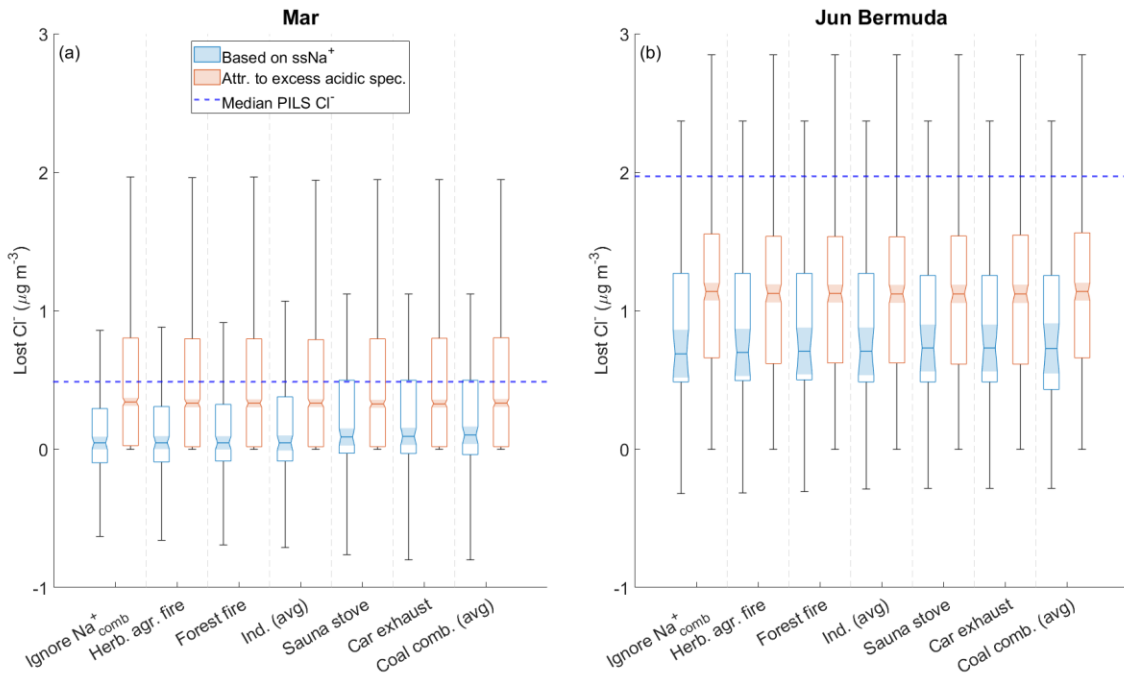
204 **Figure S10.** Relationships between mass concentration of bulk PILS Na^+ and lost Cl^- colored by
 205 bulk PILS Ca^{2+} mass concentration for the (a) December–February, (b) March, (c) March transit,
 206 (d) May, (e) May transit, and (f) June Bermuda categories.



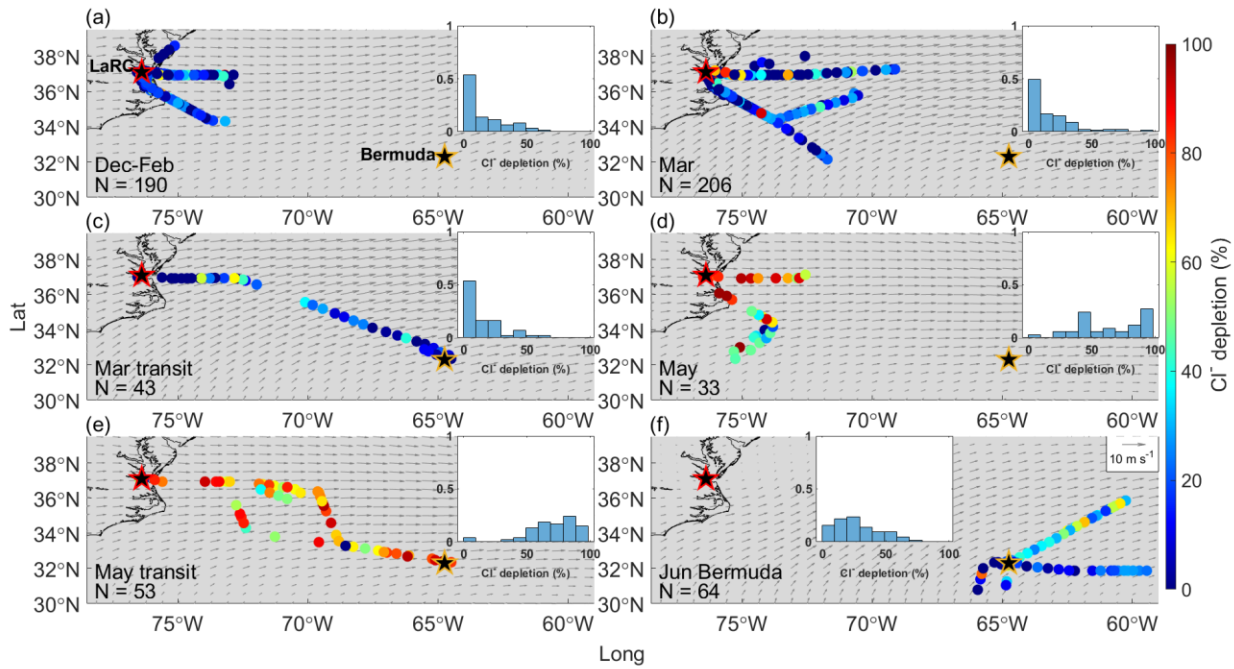
207

208 **Figure S11.** Same as Fig. S10, except colored by bulk PILS K⁺ mass concentration.

209



210 **Figure S12.** Notched box plots showing the sensitivity in actual and theoretical lost Cl⁻ to
211 accounting for Na⁺ from dust and various combustion processes during flights in **(a)** March near
212 the East Coast and **(b)** during the June field campaign in Bermuda. Light blue boxes represent
213 the actual Cl⁻ displaced from sea salt particles based on derived mass concentrations of ssNa⁺,
214 while light red boxes represent the theoretical Cl⁻ that could have been displaced by the derived
215 mass concentrations of excess acidic species. Combustion processes were assumed to not
216 contribute to bulk PILS Na⁺ mass concentrations for the "Ignore Na⁺_{comb}" results represented by
217 the pair of boxes farthest to the left in each panel. The remaining pairs of boxes are for the
218 Na⁺:K⁺ ratios described in Table S3 used to derive actual and theoretical lost Cl⁻. Note that
219 "Herb. agr. fire" above stands for "Herbaceous agricultural fire." The solid red line in the center
220 of each box indicates the median, box edges represent the 25th and 75th percentiles, and the lower
221 and upper whiskers indicate the lower limit (first quartile - 1.5 × interquartile range) and upper
222 limit (third quartile + 1.5 × interquartile range), respectively. The notches span the 95th
223 confidence interval for the median. The horizontal dashed blue lines indicate the median bulk
224 PILS Cl⁻ mass concentration for each category.



225

226 **Figure S13.** Same as Fig. S4, except for %Cl⁻ depletion.

227 **References**

- 228 Aldhaif, A. M., Lopez, D. H., Dadashazar, H., and Sorooshian, A.: Sources, frequency, and
229 chemical nature of dust events impacting the United States East Coast, *Atmospheric*
230 *Environment*, 231, 117456, <https://doi.org/10.1016/j.atmosenv.2020.117456>, 2020.
- 231 AzadiAghdam, M., Braun, R. A., Edwards, E.-L., Bañaga, P. A., Cruz, M. T., Betito, G.,
232 Cambaliza, M. O., Dadashazar, H., Lorenzo, G. R., Ma, L., MacDonald, A. B., Nguyen, P.,
233 Simpas, J. B., Stahl, C., and Sorooshian, A.: On the nature of sea salt aerosol at a coastal
234 megacity: Insights from Manila, Philippines in Southeast Asia, *Atmospheric Environment*, 216,
235 116922, <https://doi.org/10.1016/j.atmosenv.2019.116922>, 2019.
- 236 Becagli, S., Proposito, M., Benassai, S., Gragnani, R., Magand, O., Traversi, R., and Udisti, R.:
237 Spatial distribution of biogenic sulphur compounds (MSA, nssSO₄²⁻) in the northern Victoria
238 Land–Dome C–Wilkes Land area, East Antarctica, *Annals of Glaciology*, 41, 23–31,
239 <https://doi.org/10.3189/172756405781813384>, 2005.
- 240 Bondy, A. L., Wang, B., Laskin, A., Craig, R. L., Nhliziyo, M. V., Bertman, S. B., Pratt, K. A.,
241 Shepson, P. B., and Ault, A. P.: Inland Sea Spray Aerosol Transport and Incomplete Chloride
242 Depletion: Varying Degrees of Reactive Processing Observed during SOAS, *Environ. Sci.
243 Technol.*, 51, 9533–9542, <https://doi.org/10.1021/acs.est.7b02085>, 2017.
- 244 Boreddy, S. K. R. and Kawamura, K.: A 12-year observation of water-soluble ions in TSP
245 aerosols collected at a remote marine location in the western North Pacific: an outflow region of
246 Asian dust, *Atmospheric Chemistry and Physics*, 15, 6437–6453, [https://doi.org/10.5194/acp-15-6437-2015](https://doi.org/10.5194/acp-15-
247 6437-2015), 2015.
- 248 Bowen, H. J. M.: Environmental chemistry of the elements, Academic Press, London, New
249 York, xv, 333 pp., 1979.
- 250 Corral, A. F., Braun, R. A., Cairns, B., Gorooh, V. A., Liu, H., Ma, L., Mardi, A. H., Painemal,
251 D., Stamnes, S., van Diedenhoven, B., Wang, H., Yang, Y., Zhang, B., and Sorooshian, A.: An
252 Overview of Atmospheric Features Over the Western North Atlantic Ocean and North American
253 East Coast – Part 1: Analysis of Aerosols, Gases, and Wet Deposition Chemistry, *Journal of
254 Geophysical Research: Atmospheres*, 126, e2020JD032592,
255 <https://doi.org/10.1029/2020JD032592>, 2021.
- 256 Davis, R. E., Hayden, B. P., Gay, D. A., Phillips, W. L., and Jones, G. V.: The North Atlantic
257 Subtropical Anticyclone, *Journal of Climate*, 10, 728–744, [https://doi.org/10.1175/1520-0442\(1997\)010<0728:TNASA>2.0.CO;2](https://doi.org/10.1175/1520-
258 0442(1997)010<0728:TNASA>2.0.CO;2), 1997.
- 259 Farren, N. J., Dunmore, R. E., Mead, M. I., Mohd Nadzir, M. S., Samah, A. A., Phang, S.-M.,
260 Bandy, B. J., Sturges, W. T., and Hamilton, J. F.: Chemical characterisation of water-soluble
261 ions in atmospheric particulate matter on the east coast of Peninsular Malaysia, *Atmospheric
262 Chemistry and Physics*, 19, 1537–1553, <https://doi.org/10.5194/acp-19-1537-2019>, 2019.

- 263 Feng, L., Shen, H., Zhu, Y., Gao, H., and Yao, X.: Insight into Generation and Evolution of Sea-
264 Salt Aerosols from Field Measurements in Diversified Marine and Coastal Atmospheres,
265 Scientific Reports, 7, 41260, <https://doi.org/10.1038/srep41260>, 2017.
- 266 Finlayson-Pitts, B. J. and Pitts, J. N.: CHAPTER 9 - Particles in the Troposphere, in: Chemistry
267 of the Upper and Lower Atmosphere, edited by: Finlayson-Pitts, B. J. and Pitts, J. N., Academic
268 Press, San Diego, 349–435, <https://doi.org/10.1016/B978-012257060-5/50011-3>, 2000.
- 269 Haskins, J. D., Jaeglé, L., Shah, V., Lee, B. H., Lopez-Hilfiker, F. D., Campuzano-Jost, P.,
270 Schroder, J. C., Day, D. A., Guo, H., Sullivan, A. P., Weber, R., Dibb, J., Campos, T., Jimenez,
271 J. L., Brown, S. S., and Thornton, J. A.: Wintertime Gas-Particle Partitioning and Speciation of
272 Inorganic Chlorine in the Lower Troposphere Over the Northeast United States and Coastal
273 Ocean, Journal of Geophysical Research: Atmospheres, 123, 12,897-12,916,
274 <https://doi.org/10.1029/2018JD028786>, 2018.
- 275 Heintzenberg, J., Covert, D. C., and Dingenen, R. V.: Size distribution and chemical composition
276 of marine aerosols: a compilation and review, Tellus B: Chemical and Physical Meteorology, 52,
277 1104–1122, <https://doi.org/10.3402/tellusb.v52i4.17090>, 2000.
- 278 Holland, H. D.: The chemistry of the atmosphere and oceans, New York : Wiley, 378 pp., 1978.
- 279 Huang, X., Olmez, I., Aras, N. K., and Gordon, G. E.: Emissions of trace elements from motor
280 vehicles: Potential marker elements and source composition profile, Atmospheric Environment,
281 28, 1385–1391, [https://doi.org/10.1016/1352-2310\(94\)90201-1](https://doi.org/10.1016/1352-2310(94)90201-1), 1994.
- 282 Jiang, B., Xie, Z., Lam, P. K. S., He, P., Yue, F., Wang, L., Huang, Y., Kang, H., Yu, X., and
283 Wu, X.: Spatial and Temporal Distribution of Sea Salt Aerosol Mass Concentrations in the
284 Marine Boundary Layer From the Arctic to the Antarctic, Journal of Geophysical Research:
285 Atmospheres, 126, e2020JD033892, <https://doi.org/10.1029/2020JD033892>, 2021.
- 286 Junge, C. E. and Werby, R. T.: THE CONCENTRATION OF CHLORIDE, SODIUM,
287 POTASSIUM, CALCIUM, AND SULFATE IN RAIN WATER OVER THE UNITED
288 STATES, Journal of the Atmospheric Sciences, 15, 417–425, [https://doi.org/10.1175/1520-0469\(1958\)015<0417:TCOCSP>2.0.CO;2](https://doi.org/10.1175/1520-0469(1958)015<0417:TCOCSP>2.0.CO;2), 1958.
- 290 Keene, W. C. and Savoie, D. L.: The pH of deliquesced sea-salt aerosol in polluted marine air,
291 Geophysical Research Letters, 25, 2181–2184, <https://doi.org/10.1029/98GL01591>, 1998.
- 292 Keene, W. C., Pszenny, A. A. P., Galloway, J. N., and Hawley, M. E.: Sea-salt corrections and
293 interpretation of constituent ratios in marine precipitation, Journal of Geophysical Research:
294 Atmospheres, 91, 6647–6658, <https://doi.org/10.1029/JD091iD06p06647>, 1986.
- 295 Keene, W. C., Pszenny, A. A. P., Jacob, D. J., Duce, R. A., Galloway, J. N., Schultz-Tokos, J. J.,
296 Sievering, H., and Boatman, J. F.: The geochemical cycling of reactive chlorine through the
297 marine troposphere, Global Biogeochemical Cycles, 4, 407–430,
298 <https://doi.org/10.1029/GB004i004p00407>, 1990.

- 299 Keene, W. C., Pszenny, A. A. P., Maben, J. R., Stevenson, E., and Wall, A.: Closure evaluation
300 of size-resolved aerosol pH in the New England coastal atmosphere during summer, *Journal of*
301 *Geophysical Research: Atmospheres*, 109, D23307, <https://doi.org/10.1029/2004JD004801>,
302 2004.
- 303 Keene, W. C., Stutz, J., Pszenny, A. A. P., Maben, J. R., Fischer, E. V., Smith, A. M., von
304 Glasow, R., Pechtl, S., Sive, B. C., and Varner, R. K.: Inorganic chlorine and bromine in coastal
305 New England air during summer, *Journal of Geophysical Research: Atmospheres*, 112, D10S12,
306 <https://doi.org/10.1029/2006JD007689>, 2007.
- 307 Klopper, D., Formenti, P., Namwoonde, A., Cazaunau, M., Chevaillier, S., Feron, A., Gaimoz,
308 C., Hease, P., Lahmudi, F., Mirande-Bret, C., Triquet, S., Zeng, Z., and Piketh, S. J.: Chemical
309 composition and source apportionment of atmospheric aerosols on the Namibian coast,
310 *Atmospheric Chemistry and Physics*, 20, 15811–15833, <https://doi.org/10.5194/acp-20-15811-2020>, 2020.
- 312 Lamberg, H., Nuutinen, K., Tissari, J., Ruusunen, J., Yli-Pirilä, P., Sippula, O., Tapanainen, M.,
313 Jalava, P., Makkonen, U., Teinilä, K., Saarnio, K., Hillamo, R., Hirvonen, M.-R., and Jokiniemi,
314 J.: Physicochemical characterization of fine particles from small-scale wood combustion,
315 *Atmospheric Environment*, 45, 7635–7643, <https://doi.org/10.1016/j.atmosenv.2011.02.072>,
316 2011.
- 317 Manders, A. M. M., Schaap, M., Querol, X., Albert, M. F. M. A., Vercauteren, J., Kuhlbusch, T.
318 A. J., and Hoogerbrugge, R.: Sea salt concentrations across the European continent, *Atmospheric*
319 *Environment*, 44, 2434–2442, <https://doi.org/10.1016/j.atmosenv.2010.03.028>, 2010.
- 320 Murphy, D. M., Froyd, K. D., Bian, H., Brock, C. A., Dibb, J. E., DiGangi, J. P., Diskin, G.,
321 Dollner, M., Kupc, A., Scheuer, E. M., Schill, G. P., Weinzierl, B., Williamson, C. J., and Yu, P.:
322 The distribution of sea-salt aerosol in the global troposphere, *Atmospheric Chemistry and*
323 *Physics*, 19, 4093–4104, <https://doi.org/10.5194/acp-19-4093-2019>, 2019.
- 324 Nolte, C., Bhave, P., Arnold, J., Dennis, R., Zhang, K., and Wexler, A.: Modeling urban and
325 regional aerosols—Application of the CMAQ-UCD Aerosol Model to Tampa, a coastal urban
326 site, *Atmospheric Environment*, 42, 3179–3191, <https://doi.org/10.1016/j.atmosenv.2007.12.059>,
327 2008.
- 328 Ondov, J. M., Choquette, C. E., Zoller, W. H., Gordon, G. E., Biermann, A. H., and Heft, R. E.:
329 Atmospheric behavior of trace elements on particles emitted from a coal-fired power plant,
330 *Atmospheric Environment*, 23, 2193–2204, [https://doi.org/10.1016/0004-6981\(89\)90181-9](https://doi.org/10.1016/0004-6981(89)90181-9),
331 1989.
- 332 Ooki, A., Uematsu, M., Miura, K., and Nakae, S.: Sources of sodium in atmospheric fine
333 particles, *Atmospheric Environment*, 36, 4367–4374, [https://doi.org/10.1016/S1352-2310\(02\)00341-2](https://doi.org/10.1016/S1352-2310(02)00341-2), 2002.
- 335 Pilson, M. E. Q.: An Introduction to the Chemistry of the Sea, 1st ed., Prentice Hall, 1998.

- 336 Prospero, J. M.: Mineral and sea salt aerosol concentrations in various ocean regions, Journal of
337 Geophysical Research: Oceans, 84, 725–731, <https://doi.org/10.1029/JC084iC02p00725>, 1979.
- 338 Quinn, P. K. and Bates, T. S.: Regional aerosol properties: Comparisons of boundary layer
339 measurements from ACE 1, ACE 2, Aerosols99, INDOEX, ACE Asia, TARFOX, and NEAQS,
340 Journal of Geophysical Research: Atmospheres, 110, D14202,
341 <https://doi.org/10.1029/2004JD004755>, 2005.
- 342 Quinn, P. K., Coffman, D. J., Bates, T. S., Miller, T. L., Johnson, J. E., Voss, K., Welton, E. J.,
343 and Neusüss, C.: Dominant aerosol chemical components and their contribution to extinction
344 during the Aerosols99 cruise across the Atlantic, Journal of Geophysical Research: Atmospheres,
345 106, 20783–20809, <https://doi.org/10.1029/2000JD900577>, 2001.
- 346 Riley, J. P. and Chester, R. (Eds.): Copyright, in: Chemical Oceanography (Second Edition),
347 Academic Press, iv, <https://doi.org/10.1016/B978-0-12-588606-2.50002-3>, 1976.
- 348 Scheff, P. A. and Valiozis, C.: Characterization and source identification of respirable particulate
349 matter in Athens, Greece, Atmospheric Environment. Part A. General Topics, 24, 203–211,
350 [https://doi.org/10.1016/0960-1686\(90\)90457-X](https://doi.org/10.1016/0960-1686(90)90457-X), 1990.
- 351 Seinfeld, J. H. and Pandis, S. N.: Atmospheric Chemistry and Physics: From Air Pollution to
352 Climate Change, John Wiley & Sons, 1146 pp., 2016.
- 353 Shinozuka, Y., Clarke, A. D., Howell, S. G., Kapustin, V. N., and Huebert, B. J.: Sea-salt vertical
354 profiles over the Southern and tropical Pacific oceans: Microphysics, optical properties, spatial
355 variability, and variations with wind speed, Journal of Geophysical Research: Atmospheres, 109,
356 D24201, <https://doi.org/10.1029/2004JD004975>, 2004.
- 357 Spada, M., Jorba, O., Pérez García-Pando, C., Janjic, Z., and Baldasano, J. M.: On the evaluation
358 of global sea-salt aerosol models at coastal/orographic sites, Atmospheric Environment, 101, 41–
359 48, <https://doi.org/10.1016/j.atmosenv.2014.11.019>, 2015.
- 360 Stumm, W. and Morgan, J. J. aut: Aquatic chemistry : an introd. emphasizing chemical equilibria
361 in natural waters, New York [u.a.] : Wiley, 804 pp., 1981.
- 362 Turn, S. Q., Jenkins, B. M., Chow, J. C., Pritchett, L. C., Campbell, D., Cahill, T., and Whalen,
363 S. A.: Elemental characterization of particulate matter emitted from biomass burning: Wind
364 tunnel derived source profiles for herbaceous and wood fuels, Journal of Geophysical Research:
365 Atmospheres, 102, 3683–3699, <https://doi.org/10.1029/96JD02979>, 1997.
- 366 Wai, K.-M. and Tanner, P. A.: Wind-dependent sea salt aerosol in a Western Pacific coastal area,
367 Atmospheric Environment, 38, 1167–1171, <https://doi.org/10.1016/j.atmosenv.2003.11.007>,
368 2004.
- 369 Watson, J. G., Chow, J. C., and Houck, J. E.: PM2.5 chemical source profiles for vehicle
370 exhaust, vegetative burning, geological material, and coal burning in Northwestern Colorado
371 during 1995, Chemosphere, 43, 1141–1151, [https://doi.org/10.1016/S0045-6535\(00\)00171-5](https://doi.org/10.1016/S0045-6535(00)00171-5),
372 2001.

- 373 Wilson, T. R. S.: Salinity and the major elements of sea water, in: Chemical Oceanography, vol.
374 1, Academic, Orlando, FL, USA, 365–413, 1975.
- 375 Yao, X. and Zhang, L.: Chemical processes in sea-salt chloride depletion observed at a Canadian
376 rural coastal site, *Atmospheric Environment*, 46, 189–194,
377 <https://doi.org/10.1016/j.atmosenv.2011.09.081>, 2012.
- 378 Zhao, Y. and Gao, Y.: Acidic species and chloride depletion in coarse aerosol particles in the US
379 east coast, *Science of The Total Environment*, 407, 541–547,
380 <https://doi.org/10.1016/j.scitotenv.2008.09.002>, 2008.
- 381 Zhuang, H., Chan, C. K., Fang, M., and Wexler, A. S.: Formation of nitrate and non-sea-salt
382 sulfate on coarse particles, *Atmospheric Environment*, 33, 4223–4233,
383 [https://doi.org/10.1016/S1352-2310\(99\)00186-7](https://doi.org/10.1016/S1352-2310(99)00186-7), 1999.

384